

Tau Neutrinos in IceCube

Dissertation
zur Erlangung des akademischen Grades
doctor rerum naturalium
(Dr. rer. nat.)

im Fach: Physik
Spezialisierung: Experimentalphysik

eingereicht an der
Mathematisch-Naturwissenschaftlichen Fakultät
der Humboldt-Universität zu Berlin

von
Neha Lad M. Sc.
geboren am 18. April 1995

Präsidentin der Humboldt-Universität zu Berlin
Prof. Dr. Julia von Blumenthal

Dekanin der Mathematisch-Naturwissenschaftlichen Fakultät
Prof. Dr. Caren Tischendorf

Copyright Notice

This book is released into the public domain using the CC-BY-4.0 code.

To view a copy of the CC-BY-4.0 code, visit:

<https://creativecommons.org/licenses/by/4.0/>

Colophon

This document was typeset with the help of KOMA-Script and L^AT_EX using the open-source kaobook template class.

The source code of this thesis is available at:

https://github.com/LeanderFischer/phd_thesis

Abstract

In icecube, we have many neutrinos, select some very high energy ones, spend 1 year with them to group them in three flavour categories. I guess we will learn something about where they came from by doing this. Pretty normal stuff, not at all racist.

Zusammenfassung

Im IceCube haben wir viele Neutrinos, von denen wir einige mit sehr hoher Energie auswählen, verbringen 1 Jahr mit ihnen, um sie in drei Geschmackskategorien einzuteilen. Ich vermute, dass wir auf diese Weise etwas darüber erfahren, woher sie kommen. Ziemlich normales Zeug, ganz und gar nicht rassistisch.

Contents

Abstract	iii
Zusammenfassung	v
Contents	vii
1 Event Sample,(Re)construction and Particle Identification	1
1.1 Monte Carlo Simulation	1
1.1.1 Icecube simulation chain	1
1.1.2 SnowStorm Simulation	5
1.2 High Energy Starting Event (HESE) sample	6
1.3 Maximum Likelihood Event Reconstruction	8
1.4 Particle Identification of High Energy Neutrinos	10
1.4.1 Reclassification of PeV Double Cascades	14
1.4.2 Tau Polarisation	15
1.4.3 Glashow Cross-Section correction	15
1.5 Influence of South Pole Ice properties on Double Cascades Reconstruction	16
2 Sensitivity of IceCube-Gen2 to measure flavour composition of Astrophysical Neutrinos	19
2.1 IceCube Gen2	19
2.2 Simulation	20
2.2.1 Isotropic Sensor	21
2.2.2 Event Selection	22
2.3 Analysis tool : <code>toise</code>	24
2.4 Result of Flavour Sensitivity Measurements	25
APPENDIX	31
Figures	33
Tables	35
Bibliography	37

Event Sample,(Re)construction and Particle Identification

1

In the previous chapters, high-energy neutrino interactions within IceCube was discussed, focusing on how the secondary particles generated from these interactions propagate through the ice. From this, one could deduce that different neutrino flavours can create distinct morphological patterns due to the variety of charged particles produced in the interaction processes. As mentioned in Section ??, these morphological signatures are crucial in identifying the neutrino flavour, although it becomes particularly challenging in the case of tau neutrino-induced double-bang events. Apart from the complexities of reconstruction, another critical aspect is the selection of astrophysical neutrinos from the overwhelming background of atmospheric muons and neutrinos.

In this chapter, the high-energy neutrino sample used for the analysis presented in this thesis will be detailed, along with the reconstruction method used to identify the particles based on the event's morphology. The chapter will begin with a general overview of the simulation chain in IceCube, followed by a brief overview of the SnowStorm simulations used for the analysis. Lastly, the chapter will discuss the influence of the South Pole IceModel on reconstructed Double Cascade events.

1.1 Monte Carlo Simulation

The hunt for astrophysical neutrino interactions in the IceCube detector is conducted without access to actual data, a method known as **blind analysis**. To develop the selection (rejection) criteria for signal (background) events, and their light yield reconstruction, simulated events are used.¹ By comparing the distribution of an observable quantity between simulated and real data events, conclusions can be drawn about the detected neutrino population. Hence, simulating how IceCube responds to neutrinos and other particles is essential for comprehending the collected data.

Event simulation in IceCube is based on commonly used Monte Carlo methods. The simulation framework covers all stages, from the generation and propagation of a primary particle to the emission and propagation of Cherenkov light, and finally, the digitized waveforms recorded by all hit DOMs in IceCube.

1.1.1 Icecube simulation chain

The IceCube simulation begins with a *particle generator* that simulates a flux of particles hitting the detector. The primary particle can be a neutrino or a cosmic ray particle reaching Earth's atmosphere. Neutrinos may reach the detector directly, while cosmic rays interact with particles in the atmosphere to produce a shower of particles, from which muons and neutrinos can reach the detector by propagating through ice, forming the so-called atmospheric neutrino and atmospheric muon background.

1.1 Monte Carlo Simulation	1
1.1.1 Icecube simulation chain	1
1.1.2 SnowStorm Simulation	5
1.2 High Energy Starting Event (HESE) sample	6
1.3 Maximum Likelihood Event Reconstruction	8
1.4 Particle Identification of High Energy Neutrinos	10
1.4.1 Reclassification of PeV Double Cascades	14
1.4.2 Tau Polarisation	15
1.4.3 Glashow Cross-Section correction	15
1.5 Influence of South Pole Ice properties on Double Cascades Reconstruction	16

1: In some cases, typically during the development phase of the analysis sample, selection cuts are validated on small subset (10%) of the experimental data, known as *the burn sample*.

Particle Generation

2: a probability that gets stored as propagation weight for each stage and enters in total weight calculations as a *total interaction probability*.

[1]: Dziewonski et al. (1981), *Preliminary reference earth model*

[2]: Halzen et al. (1998), *Tau-neutrino appearance with a 1000 megaparsec baseline*

The software that generates neutrinos is called NuGen (Neutrino Generator) and is based on ANIS (All Neutrino Interaction Simulation). To start the simulation, neutrinos of a selected flavour are drawn from a power-law energy spectrum with an equal probability of being a neutrino or antineutrino. Neutrino directions are sampled from an isotropic distribution and aimed to intersect with an imaginary surface centered on the detector. Each neutrino is then propagated in discrete steps through matter encountered on the way to the detector. For each step, a neutrino interacts with a probability² of $1 - e^{-\sigma n \Delta x}$, where σ is the total interaction cross-section and n is the density of nucleons at the location in the Earth. The nucleon density is modelled using the *Preliminary Earth Reference Model (PREM)* [1], which provides the mass density of the Earth as a function of radius. Because the tau has a short lifetime and a large radiation length, it usually transfers a significant portion of its energy to the tau neutrino produced in its decay (see Section ??). This leads to substantial decrease of overall ν_τ flux at higher energies, a phenomenon known as *tau-regeneration* [2]. This so-called earth effect is also taken into account by the NuGen software.

After enough steps, neutrinos will reach the imaginary cylinder defining the detection volume where they are forced to interact somewhere between the projected entry and exit points of the cylinder according to a uniform distribution. In the case of a muon resulting from a CC ν_μ interaction far outside the surface, the length at which interactions are required to occur is automatically extended backward based on a parameterization of the muon range in ice. When a neutrino interaction is forced, a weight of $p_{\text{int}} = n\sigma L \exp(-n\sigma L_{\text{before}})$ must be assigned, where L_{before} is the distance before the selected interaction point where an interaction may have occurred, and L is the total length where an interaction may have occurred. This weight is often combined with the propagation weight to give a total interaction probability weight $w_{\text{int}} = p_{\text{prop}} p_{\text{int}}$. The interaction type is then randomly selected according to CC, NC, and GR cross-sections, and secondary particles are generated for further propagation by another program. In IceCube, single atmospheric and astrophysical neutrinos cannot be distinguished on an event-by-event basis. Therefore, the NuGen-generated neutrinos are used for both atmospheric and astrophysical fluxes. Neutrinos will have weights assigned to them according to the expected (or tested) atmospheric and astrophysical fluxes, and these weights can be used to calculate an expected event rate.

[3]: Heck et al. (1998), CORSIKA: A Monte Carlo code to simulate extensive air showers

To generate atmospheric muons and neutrinos, an adapted version of CORSIKA [3] is used to simulate the production of muons resulting from cosmic ray showers in the Earth's atmosphere. This process begins with a primary particle, typically a nucleus, initiating a cascading shower of particles upon interaction with the atmosphere. Only neutrinos and muons from these showers are capable of reaching the detector. Due to the impracticality of simulating atmospheric neutrino interactions using CORSIKA, only the muons generated in the showers are transmitted to the detector. The software allows for event weighting based on various cosmic ray models. CORSIKA is currently the exclusive software capable of producing muon bundles, which are large numbers of muons origi-

nating from the same cosmic ray shower. However, a major limitation of CORSIKA is its computational expense, as it propagates all particles from a cosmic ray shower, most of which are undetectable in a sub-surface detector like IceCube. To address this drawback, MUONGUN [4] was developed to simulate single muons more efficiently and economically by generating them directly around the detector volume. In the context of HESE (which will be discussed in Section 1.2), the primary background arises from single muons, as muon bundles produce a more continuous light deposition, resulting in a higher likelihood of being vetoed upon entering the detector. Since flux models more complex than a simple power law are often required, NuGen simulations can be re-weighted to match any arbitrary flux. A weight is assigned to each event that reflects the ratio between the desired flux $n_{\text{expected}} = \Phi(E)$ and the generated fluence of neutrinos. The generated fluence can be expressed as,

$$n_{\text{generated}} = \frac{N(E)}{\Omega A_{\perp}} \quad (1.1)$$

where A_{\perp} is the projected area of the detection surface for each neutrino, and Ω is the solid angle covered by the simulation, typically 4π for neutrinos coming from the entire sky. $N(E)$ represents the energy distribution of simulated neutrinos, which, for a power-law distribution with N_0 events and a power-law index γ , spanning from energy E_{\min} to E_{\max} , is given by:

$$N(E) = \frac{N_0 E^{-\gamma}}{\int_{E_{\min}}^{E_{\max}} E^{-\gamma} dE} \quad (1.2)$$

Here, N_0 refers to the number of neutrino or antineutrino events, and not the total, when separate fluxes for neutrinos and antineutrinos are known. This implies that N_0 represents half of the total number of events generated for each neutrino flavor. Finally, accounting for the interaction weight, the total weight assigned to each neutrino (in units of Hz) is:

$$\begin{aligned} w &= w_{\text{int}} \frac{n_{\text{expected}}}{n_{\text{generated}}} \\ &= w_{\text{int}} \frac{A_{\perp} \Omega \Phi(E)}{N(E)} \end{aligned} \quad (1.3)$$

By summing these weights over all simulated events that pass the event selection, the expected event rate for any desired flux model can be calculated.

Secondary Charged Particle Propagation

Once a particle interaction occurs within the detector volume, the next step is to generate and propagate secondary particles through the ice. Depending on their nature, these secondary particles may undergo further interactions within the ice, with some of them producing detectable Cherenkov light in the detector volume (see Section ?? for details). Both atmospheric muons from air showers and secondary leptons, such as electrons, muons, and taus from CC neutrino interactions, are propagated

[4]: Santen (2014), *Neutrino Interactions in IceCube above 1 TeV: Constraints on Atmospheric Charmed-Meson Production and Investigation of the Astrophysical Neutrino Flux with 2 Years of IceCube Data taken 2010–2012*

a block diagram of simulation chain here

[5]: Koehne et al. (2013), *PROPOSAL: A tool for propagation of charged leptons*

[6]: Chirkin et al. (2004), *Propagating leptons through matter with Muon Monte Carlo (MMC)*

[7]: Voigt (2008), *Sensitivity of the IceCube detector for ultra-high energy electron-neutrino events*

[8]: Radel et al. (2013), *Calculation of the Cherenkov light yield from electromagnetic cascades in ice with Geant4*

[9]: Rädel et al. (2012), *Calculation of the Cherenkov light yield from low energetic secondary particles accompanying high-energy muons in ice and water with Geant 4 simulations*

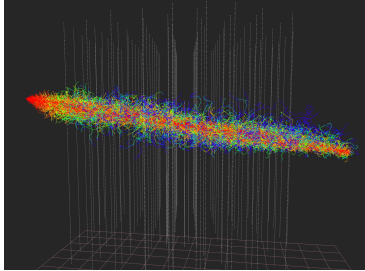


Figure 1.1: Light emission pattern of a simulated muon track event, using the direction propagation program `CLSim`. The colored lines show individual photon paths through ice, with red indicating earlier and blue indicating later compared to an unscattered photon. Figure taken from [10]

[11]: Kopper (n.d.), *Clsim*

[12]: Chirkin (2013), *Photon tracking with GPUs in IceCube*

3: Three for the source position, three for the DOM position, two for the light source orientation, and one for time.

through the ice after they are produced. The software used for lepton propagation is called PROPOSAL (Propagator with Optimal Precision and Optimized Speed for All Leptons) [5] and is based on the previous implementation MMC (Muon Monte Carlo) [6]. The lepton production is simplified by assuming that the emission angle is aligned with the incident angle of the primary particle, and that it travels at the speed of light, which are both reasonable assumptions above the energy threshold of 100 GeV. The various propagation effects of different particle types and energies, as described in ??, are taken care of by PROPOSAL. In particular, highly energetic muons are simulated to have long tracks that are predominantly characterized by stochastic energy losses. Electromagnetic and hadronic cascades, as described in Section ??, are simulated by CMC (Cascade Monte Carlo) [7]. It generates individual particle showers by randomly sampling energy losses from the energy-dependent shower parametrization and also takes the LPM-effect into account. The shower parametrizations have been determined by fitting the Cherenkov light yield for a full shower simulation using GEANT4 (Geometry And Tracking) [8, 9].

Photon Propagation

Once all primary and secondary particles have traversed the detector, the next phase of the simulation process involves the emission and propagation of Cherenkov photons from all visible particles or energy losses (as discussed in Section ??). The number of cherenkov photons is proportional to the combined track length of all charged particles, and the refraction index of ice. Individual photon propagation is traced through an OpenCL-based photon-tracking simulation (as shown in Figure 1.1), known as `CLSim` [11], derived from *Photon Propagation Code* (PPC) [12]. The SPICE models (as detailed in Section ??) are used to describe the scattering and absorption of photons. Each photon is tracked through multiple scatterings until it either reaches the collection area of a DOM or, more often, is absorbed. `CLSim` harnesses GPUs for photon propagation due to their efficiency in running numerous simple operations (such as photon scattering) in parallel [12].

Since the direct propagation of photons even by using GPUs can be extremely time and power consuming, an alternative method is used in IceCube that creates a look-up table that stores the expected timing distribution of photoelectrons at a Digital Optical Module (DOM) for various configurations of the light source and DOM. The concept involves simulating a light source (cascade, track, or flasher) at specific depths and directions multiple times, while tracking the photon yield around the source. Initially, the challenge of creating this table seemed daunting due to the complexity of the problem, as it required a table with 9 dimensions³. However, One can take advantage of the approximate horizontal translational and azimuthal symmetry of the ice to reduce the dimensions to 6: depth of the source in ice, zenith angle of the source, displacement vector of the DOM from the source, and time. It is important to note that this approach has its limitations, as it disregards certain effects such as ice layer tilt and anisotropic scattering, which do not adhere to the symmetry assumptions. In recent years, these limitations have been overcome by introducing corrections to scattering lengths (the

so-called *effective distance correction*), which was done while developing the double cascade reconstruction [13] that will be explained in Section 1.4, and also by introducing corrections directly in modelling of the ice to account for ice anisotropy and tilt corrections, see Section ?? for details. Initially, Photonics was used to predict and store the expected photon flux in a multi-dimensional histogram structure, but this method had drawbacks such as binning issues and inaccuracies at great distances. Currently, a more effective approach involves fitting the photoelectron distribution obtained from CLSim or PPC to a tensor product B-spline surface [14]. This offers the advantage of having a smooth function of all 6 coordinates and can address unphysical fluctuations caused by limited statistics through the use of regularization.

[13]: Usner (2018), *Search for Astrophysical Tau-Neutrinos in Six Years of High-Energy Starting Events in the IceCube Detector*

Detector Simulation

The detector's response is the final step in the simulation process. The PMT's sensitivity depends on the wavelength and angle of the incoming photon, as well as its quantum efficiency. This means that not every photon will trigger the PMT. The simulation takes into account the varying PMT sensitivity for each photon. Additionally, the simulation considers the angular acceptance of photons, accounting for local scattering variations in the ice. The PMT hardware has been thoroughly calibrated and studied in the lab [15], and these results have been incorporated into the simulation. It's important to model the transit time and jitter of the PMT in the simulation, as these factors affect the timing and width of the pulse. Furthermore, all triggers used in real-time data collection at the South Pole are also included in the simulation. This final step in the simulation process completes the creation of a simulated event.

[14]: Whitehorn et al. (2013), *Penalized splines for smooth representation of high-dimensional Monte Carlo datasets*

1.1.2 SnowStorm Simulation

As described in previous section, specifically for photon propagation stage precise knowledge of ice is important. While we use calibration measurements to estimate the detector properties, this only provides limited precision. When conducting simulations, which are crucial for estimating the detector's response, one need to be careful not to assume specific detector properties. For most of the IceCube analyses so far, variations of the detector response were included using a particular strategy: A set of Monte Carlo simulations with *baseline* values of all systematic parameters was created to estimate event rate in the analysis. The baseline value of a systematic parameter is its most likely value determined from calibration. Variations of this baseline event rate caused by a different, *off-baseline*, detector response were estimated using different *discrete systematics sets*. The combination of discrete baseline and systematics sets allows the estimation of the analysis variables as well as their variation with the detector systematics. This variation is typically assumed to be small and estimated with a low-order Taylor expansion. The off-baseline systematics sets are then used to estimate the coefficients of this expansion.

A new approach to model detector systematic uncertainties has been developed in IceCube called, **SnowStorm Method** [16]. The significant difference compared to the discrete systematics approach described above

[15]: Abbasi et al. (2010), *Calibration and characterization of the IceCube photomultiplier tube*

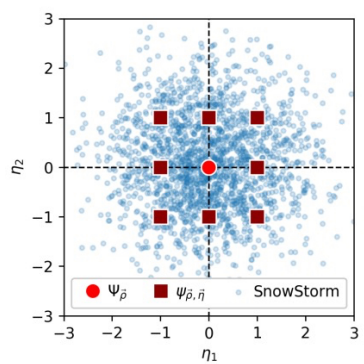


Figure 1.2: Illustration of the SnowStorm method described in the text. It depicts the contrast between numerous discrete shifts in nuisance parameters (indicated by red squares), each necessitating an entire Monte Carlo set, in comparison to a single SnowStorm Monte Carlo (represented by small blue dots). Figure taken from [16]

[16]: Aartsen et al. (2019), *Efficient propagation of systematic uncertainties from calibration to analysis with the SnowStorm method in IceCube*

is that each detector systematic parameter continuously varied while generating the MC events, as visualized in Figure 1.2. Using the SnowStorm method, one obtains a single MC set representing all variations in the detector response. This can help an analysis by reducing the bookkeeping effort necessary for using multiple discrete sets, studying variations in a large number of detector systematic parameters at once without loss in statistics, and allowing analyses of different event selections to use the same MC set and "marginalize" over all detector systematic parameters that are not relevant for a single analysis.

The analysis presented in this thesis uses simulations generated using this aforementioned novel method. It involves uniform and independent sampling distributions for all relevant parameter uncertainties in the flavor analysis. These simulations cover all three flavors of neutrinos and were created using the SPICE-3.2.1 icemodel. They were designed for general use and were also utilized by several other IceCube analyses simultaneously, see [17] and [18] for details. The simulation sets were developed for primary neutrinos in the energy range of $E_\nu = [100 \text{ GeV} - 1 \text{ PeV}]$ assuming a single power law of $E_\nu^{-1.5}$, and in the range [1-100 PeV] with a E_ν^{-1} spectrum. The harder spectrum is generally chosen, particularly for higher energy datasets, to ensure a sufficiently large number of events at those energies. Using the weighting method described previously, one can reweight the neutrino events to match any desired spectrum.

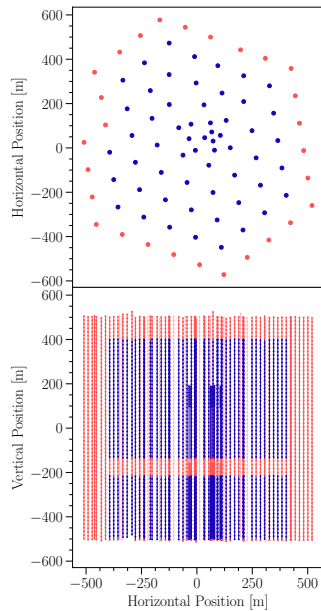


Figure 1.3: The top view (above) and side view (below) display the veto DOMs and the DOMs within the fiducial volume for HESE. DOMs highlighted in red represent the veto region, while those in blue define the fiducial volume. Events where the initial detected light comes from the veto region are excluded from the analysis. Figure taken from [19].

[20]: Aartsen et al. (2013), *Evidence for High-Energy Extraterrestrial Neutrinos at the IceCube Detector*

[19]: Abbasi et al. (2021), *IceCube high-energy starting event sample: Description and flux characterization with 7.5 years of data*

[21]: Abbasi et al. (2022), *Detection of astrophysical tau neutrino candidates in IceCube*

1.2 High Energy Starting Event (HESE) sample

The High Energy Starting Events (HESE) selection is a comprehensive, all-sky, all-flavor sample of astrophysical and atmospheric neutrinos observed in IceCube. This selection process led to IceCube's first significant milestone: the discovery of an astrophysical neutrino flux [20]. Subsequently, a particle identifier was developed using this sample with added years of data, eventually finding two tau neutrino candidates in IceCube [19, 21]. For the analysis presented in this thesis, this sample was again used, along with some updates in Self-Veto calculations, that shall be introduced in Section 1.2. The concept behind HESE is to establish a veto region on the detector's outer edges to select only events where the initial Cherenkov photons are detected inside the fiducial volume. As shown in Figure 1.3, the veto region includes the outer strings, a top layer of 90 m, a central layer of 80 m around the dust layer, and a 10 m bottom layer. The very thicker veto at the top is essential for filtering out atmospheric muons entering from above. However, the veto can be thinner at the bottom of the detector since up-going atmospheric muons do not exist. The inclusion of a veto around the dust layer is crucial, as horizontal events passing through this highly absorptive region can mimic starting events. To pass the veto, events must deposit fewer than 3 photoelectron (PE) in the veto region out of the first 250 PE recorded within the fiducial volume, and a minimum total charge of 6000 PE is required to ensure high-energy events are selected.

The HESE selection is particularly powerful due to its simplicity, as it does not rely on complex reconstructions, making it robust against changes in filtering or reconstruction algorithms. The fact that it is an all-flavour

sample, can help break degeneracies caused by different neutrino flavors producing similar event patterns. Additionally, the all-sky nature of HESE allows for the study of the zenith distribution of events, which can distinguish between atmospheric and astrophysical neutrinos. However, HESE does have limitations: the high-energy threshold introduces uncertainty in estimating background contributions and astrophysical parameters, and the veto region reduces the detector's effective volume. An extension of HESE to lower energies, known as Medium Energy Starting Events (MESE), has been developed [22] (and recently updated [23]) to overcome some of these limitations.

Despite of rejecting a significant fraction of atmospheric background, HESE retains the majority of astrophysical neutrinos within its fiducial volume. The neutrino effective area of the HESE sample, increases with neutrino energy due to the larger amount of visible light deposited (see Figure 1.11). At energies above a few hundred TeV, the effective areas become similar across all flavors, except the Glashow resonance of $\bar{\nu}_e$ at 6.3 PeV. However, at lower energies, the effective area varies by flavor due to differences in energy deposition during charged-current interactions, with electron neutrino interactions producing the highest effective area due to the nearly complete energy deposition in electromagnetic and hadronic cascades. For different zenith angles, the effective area decreases as the zenith angle increases, particularly in the up-going region at high energies. This is a result of Earth absorption, which becomes significant for neutrinos above approximately 1 PeV. The distinction between tau neutrinos and other flavors at the highest energies is due to the phenomenon of tau regeneration, where the tau neutrino regenerates after the decay of a tau lepton. Muon neutrino interactions, on the other hand, produce muons that deposit only part of their energy before escaping the detector, resulting in a higher detection threshold. Neutrino interactions, especially for ν_τ , exhibit effective areas between those of ν_μ and ν_e .

Atmospheric Neutrino Self-Veto

As mentioned in Section ??, high-energy cosmic ray showers produce many neutrinos and muons, which are the only particles able to reach underground detectors such as IceCube. When atmospheric neutrinos reach the detector, they are typically accompanied by other particles from the same CR shower, mostly muons. The chance of a detectable muon accompanied with an atmospheric neutrino is called **the atmospheric self-veto probability**. Several things affect this probability, such as the type, energy, and direction of the neutrino. In the case of high-energy CR showers, some muons may reach the detector and *trigger* the veto that marks the event as background. The likelihood of rejecting an atmospheric neutrino through this self-veto mechanism increases with higher neutrino energy and more vertical shower angles. With such a modelling, one effectively suppresses the flux of atmospheric neutrinos, in down-going region⁴. **The passing fraction** of atmospheric neutrinos—defined as the fraction that is not accompanied by a detectable muon from the same CR shower—varies with both neutrino energy and zenith angle [24]. It tends to increase at larger zenith angles, as muons must travel farther through the atmosphere to reach IceCube, as shown in Figure

[22]: Aartsen et al. (2015), *Atmospheric and astrophysical neutrinos above 1 TeV interacting in IceCube*

[23]: Basu et al. (2023), *From PeV to TeV: Astrophysical Neutrinos with Contained Vertices in 10 years of IceCube Data*

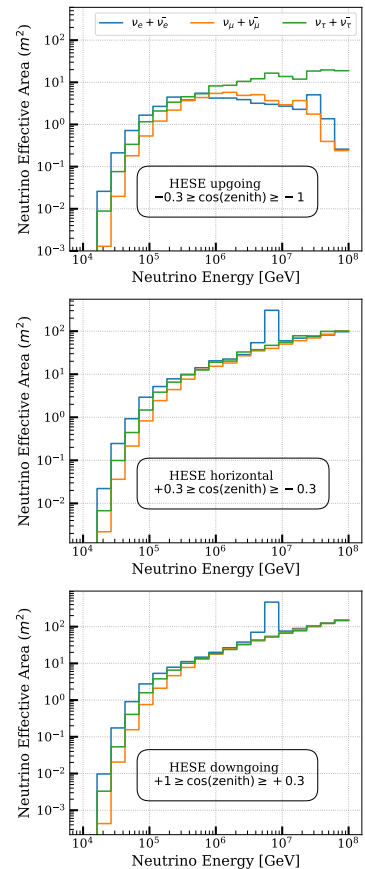


Figure 1.4: The neutrino effective areas for the high-energy starting event selection as a function of neutrino energy. The distributions are shown for all neutrino flavors, broken down by various zenith angle ranges.

4: This process only applies to downward-moving atmospheric neutrinos because muons cannot reach IceCube from below the Earth

[24]: Arguelles Delgado et al. (2018), *Unified atmospheric neutrino passing fractions for large-scale neutrino telescopes*

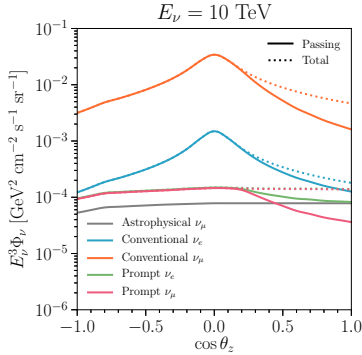


Figure 1.5: The Atmospheric neutrino fluxes at $E_\nu = 10$ TeV. The plot shows the fraction of the flux that is **not** vetoed, known as **passing fluxes** (solid lines), alongside the total flux entering the detector (dashed lines) as a function of the cosine of the zenith angle. Figure is adapted from [24].

[24]: Arguelles Delgado et al. (2018), *Unified atmospheric neutrino passing fractions for large-scale neutrino telescopes*

[25]: Yuan et al. (n.d.), *nuVeto*

[26]: Fedynitch et al. (2015), *Calculation of conventional and prompt lepton fluxes at very high energy*

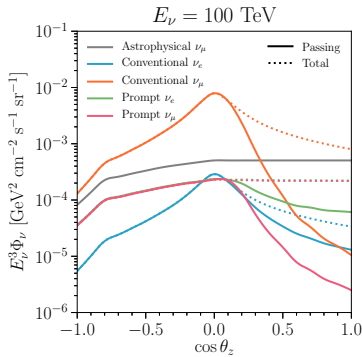


Figure 1.6: The atmospheric neutrino fluxes and the effect of self-vetoing are displayed for a neutrino energy level of $E_\nu = 100$ TeV, see caption of Figure 1.5. Figure taken from [24].

[27]: Aartsen et al. (2014), *Energy Reconstruction Methods in the IceCube Neutrino Telescope*

[14]: Whitehorn et al. (2013), *Penalized splines for smooth representation of high-dimensional Monte Carlo datasets*

[13]: Usner (2018), *Search for Astrophysical Tau-Neutrinos in Six Years of High-Energy Starting Events in the IceCube Detector*

5: to account ice layer tilt and anisotropy due to birefringence (see Section ?? for details) separately

[28]: Yuan (2023), *Detecting neutrinos in IceCube with Cherenkov light in the South Pole ice*

1.5. At neutrino energies greater than 100 TeV, the contribution from astrophysical neutrinos begins to outweigh the atmospheric background, improving IceCube’s ability to detect astrophysical neutrinos as indicated in Figure 1.6.

The passing fractions used in the analysis presented in this thesis is based on the calculations derived in [24] a formalism used in 7.5 years of HESE analysis [19] through the *nuVeto* package [25]. The previously used calculations are further updated using MCEq package, MCEQ, a tool designed to solve the cascade equations governing cosmic ray-induced showers, allowing for more precise and computationally efficient predictions of atmospheric lepton fluxes [26].

1.3 Maximum Likelihood Event Reconstruction

With the aforementioned HESE sample, next step is to infer the properties of these events—primarily energy, direction, and the deposited light pattern (morphology). To do so, it is necessary to *reconstruct* each individual event. The reconstructed properties are then used to create probability density functions (PDFs) that facilitate likelihood fits for making the desired physics measurements (as outlined in Section ??). Therefore, it is crucial to reconstruct the event properties as accurately as possible. The analysis presented here utilizes a maximum-likelihood estimation (MLE) approach, called *millipede* for event reconstruction.

millipede aims to maximize the likelihood of the observed light pattern from an event, given a specific source hypothesis. The input data comprises individual pulses detected by Digital Optical Modules (DOMs), expressed in terms of charge (measured in photoelectrons (PEs)) and time. These pulses are deconvolved from the digitized waveforms using established single-photoelectron (SPE) pulse templates. The likelihood function compares the observed data to the expected data for a given hypothesis and adjusts the parameters to maximize this likelihood, details of which can be found in [27].

The expected number of photons detected at DOM j follows a Poisson distribution characterized by a mean $\lambda_j = \Lambda_j E$, where Λ_j represents the expected photon yield from a 1 GeV cascade at DOM j , and E signifies the cascade’s energy, stored in tabulated form as photo splines [14], which were originally developed and used in an analysis similar to one presented in this thesis [13] and now have been updated with newer icemodel⁵ [28] *. The likelihood of detecting k_j photons at DOM j for a cascade with energy E is given by:

$$L_j = \frac{(E\Lambda_j)^{k_j} e^{-E\Lambda_j}}{k_j!} \quad (1.4)$$

By taking the logarithm and summing over all DOMs, including noise hits ρ_j , along with an expansion to include multiple light sources i and timing information, the log-likelihood can be expressed as:

* These updated tables are used in the analysis presented in this thesis

$$\ln L = \sum_{i,j,t} (k_{jt} \ln(E_i \Lambda_{ijt} + \rho_{jt}) - (E_i \Lambda_{ijt} + \rho_{jt}) - \ln(k_{jt}!)) \quad (1.5)$$

The hypothesis to be compared encompasses the event parameters ($x_s, y_s, z_s, t_s, \theta_s, \phi_s, E_s$), which define the source's location, time, direction, and energy respectively.

`millipede` offers a comprehensive set of configurations that allow users to define how photons are organized in terms of time bins, the magnitude of changes in various parameters, and the exclusion of specific modules from the likelihood calculation. One crucial aspect of these settings is the selection of an ice model for data reconstruction. This model plays a vital role in predicting the expected number of photons that will reach a DOM based on variables such as distance and direction from the source. Additionally, the ice model can influence the timing information of these photons [29], which is critical for accurate event reconstruction.⁶. As for exclusions of certain modules, **bright DOMs** and **Saturated DOMs** are excluded from the likelihood fit because they may introduce bias by contributing excessively to Equation 1.5. These particular DOMs generally account for a significant portion of the total observed charge. Hence, bright and saturated DOMs alongwith other DOMs that may have failed during the Run are generally labelled as *Bad DOMs* and are collectively excluded from the reconstruction. `millipede` framework helps reconstruct single and double cascades, along with track source hypotheses. Although they all use the same likelihood from Equation 1.5, they each have different ways to define sources. The hypothesis that fits the observed data best is found by comparing maximum likelihood values, which gives an idea of the interaction type in the detector.

monopod: `monopod` does a simple one-particle cascade energy fit, in other words it assumes a single light source. It minimizes parameters such as the cascade's deposited energy, neutrino direction (azimuth and zenith), cascade vertex position (x, y, z), and vertex time, represented as, $\vec{h} = (x, y, z, t, \theta, \phi, E)$ [4]. The reconstructed vertex here refers to the shower maximum, which is the peak of the longitudinal energy loss profile and is typically displaced from the interaction vertex by several meters in the considered energy range.

taupede: The double cascade fitting algorithm, `taupede`, maximizes the likelihood of two energy depositions with energy E_1 and E_2 respectively, separated by distance L_{dc} . The second cascade's direction matches the first, and its vertex is determined by the first cascade's vertex, direction, and double cascade length L_{dc} . The parameters for the double cascade hypothesis are $\vec{h} = (x_1, y_1, z_1, t_1, \theta, \phi, E_1, L_{dc}, E_2)$, with the tau traveling in the same direction as the incoming neutrino due to Lorentz boosting. The light yield and timing at each Digital Optical Module (DOM) are compared with expected values from the two energy depositions. For the second cascade's timing, the conditions are $|\vec{x}_2 - \vec{x}_1| = L_{dc}, \quad t_2 - t_1 = cL_{dc}$ ⁷.

mumillipede: Track-like events are parameterized as multiple cascades along its path. The total deposited energy is given by $E_{dep} = \sum_k E_k$. Although the deposited energy is not a reliable indicator of the primary neutrino energy, the parameters related to direction and time are vital for neutrino point-source searches.

Bright DOM

A Bright DOM generally refers to a situation where a high energy event occurs close to a string, and in first pulse itself, a large amount of charge is observed. Empirically, this *large amount of charge* is assumed to be 10 times the average observed charge of the event.

Saturated DOM

A DOM is considered saturated if its PMT reaches saturation. This can happen if an event occurs close to a string or a very high energy interaction occurs, producing many photons that gets collected by the PMT. These DOMs generally don't have a *complete* digitized waveforms, making them unsuitable to be used in likelihood based reconstruction.

[29]: Abbasi et al. (2024), *In situ estimation of ice crystal properties at the South Pole using LED calibration data from the IceCube Neutrino Observatory*

6: Different approaches to model the ice at the South Pole can significantly affect the reconstructed properties of an event, in particular the double cascade reconstruction using `taupede` (see Section 1.5 at the end of this chapter for such detailed checks)

DeepCore DOM exclusion

DeepCore DOMs have traditionally been excluded from high-energy reconstruction methods like `millipede` because it uses spline tables that assume a uniform single photoelectron (SPE) template for all DOMs. However, the higher quantum efficiency of DeepCore DOMs results in significantly different charge collection, meaning their SPE templates differ from those of other DOMs. Recent efforts have updated simulations to address this issue (as will be discussed in Section ??).

[4]: Santen (2014), *Neutrino Interactions in IceCube above 1 TeV: Constraints on Atmospheric Charmed-Meson Production and Investigation of the Astrophysical Neutrino Flux with 2 Years of IceCube Data taken 2010–2012*

7: assuming tau travels through the ice at the speed of light c .

8: All algorithms are run multiple times, starting with a provided seed, where each subsequent iteration uses the output from the previous one, as explained in Section 1.4.

[13]: Usner (2018), *Search for Astrophysical Tau-Neutrinos in Six Years of High-Energy Starting Events in the IceCube Detector*

The algorithm outlined above relies on the quality of the seed, which serves as the initial hypothesis \vec{h}_0 . This seed is adjusted until a satisfactory match is achieved between the expected and actual light yield. This process has proven challenging, especially in the case of `taupede`, where the seed combines aspects of both a cascade and a track. Locating an appropriate seed is difficult, and the reconstruction process is influenced by the choice of seed. To reduce this influence, one can either modify the seed or increase the number of iterations⁸; however, both approaches result in greater computational expenses. To tackle the challenges associated with reconstructing double cascade events, an improved method for implementing the `taupede` fit was developed [13]. This method effectively converts the fitting process into a *brute-force* approach, where multiple hypotheses are explored and evaluated.

Simple reconstruction methods like `LineFit` and `SPEFit` provide fast initial estimates for event properties. These methods use limited event information, such as the first photon arrival time or total photoelectrons, without relying on detailed ice properties. The results are then used as seeds for more refined algorithms like `millipede`. For cascade-like events, simpler MLE methods are used to find a charge-weighted mean position of the source, providing an efficient first estimate.

1.4 Particle Identification of High Energy Neutrinos

[21]: Abbasi et al. (2022), *Detection of astrophysical tau neutrino candidates in IceCube*

Event reconstruction is performed using the aforementioned `millipede` framework, which enables the identification of different interaction types by assigning a **particle identifier (PID)** to each reconstructed event. The PID provides the probability that an event corresponds to a particular type of interaction. A **ternary topology identifier** has been developed (initially developed in [13] and later used to find first two tau candidates in IceCube [21]) based on the three event topologies—single cascade, double cascade, and track. By using these IDs, Monte Carlo templates are constructed to extract the contribution fractions from each neutrino flavor (see Chapter ??).

The analysis presented in this thesis has two main goals: to identify double cascades produced by tau neutrinos and to determine the flavor composition of astrophysical neutrinos. Given the complexity of detecting double cascades and the susceptibility of the reconstruction algorithm to failures and dependence on the initial seed hypothesis, the classification process uses a combination of algorithms offered by the `millipede` framework, which run in parallel on each of the HESE events that provides likelihood for the three event morphologies.

As mentioned before, these methods are seed dependent, hence to start with, all selected HESE events are reconstructed using first-guess algorithms to determine their vertex and direction. Result of these quick methods provides an initial fit for the event’s position and trajectory, serving as a seed for `monopod`, which performs a fit with four iterations.

Generating a reliable seed for `taupede` is more complex. Multiple seeds are constructed using the `monopod` fit and generated with varying

lengths (10, 25, 50, and 100 meters), each shifted forward, backward, or centered along the direction of the seed in bruce-force way [13]. An amplitude-only `taupede` fit is performed for each of the 12 seeds⁹, and the three best-performing seeds are selected for a full fit, performing 4 iterations of fits again, which incorporates photon arrival times at the Digital Optical Modules (DOMs). This method accounts for the diverse photon arrival patterns produced by scattered photons in single energy depositions [30]. The tracks are reconstructed using the `SPEFit` algorithm, which iteratively (16 times) fits a track based on the first photo-electron detected at each DOM. Although the `mumillipede` algorithm could also reconstruct tracks, it is computationally intensive, so `SPEFit` is preferred. Finally, `mumillipede` unfolding is performed along the directions determined by each topology fit (monopod, `taupede`, and `SPEFit16`), allowing for a comparison of likelihood values for each hypothesis. The best fit is selected for final classification based on the highest likelihood value.

Since identifying tau-induced double cascades is main goal of this process, the comparisons of the three likelihoods is not the only proxy by which the classifier selects a double cascade event. First, the `taupede` fit is vetted through **Quality Criteria**, on the basis of containment, and reconstructed properties. If these criteria are satisfied¹⁰, further classification is performed using additional selection criteria based on observables derived from reconstructed quantities, described below:

The reconstructed direction of a particle is indicated by its zenith and azimuth angles. The azimuthal angle is not useful for distinguishing between atmospheric and diffuse astrophysical neutrino fluxes since both are isotropically distributed. However, it is important for addressing systematic uncertainties in reconstructed track length due to anisotropic light scattering in the ice. However, zenith angle provides a reliable estimate of the neutrino's initial trajectory, especially for tracks, which can be reconstructed more accurately than cascades.

The total deposited energy (E_{tot}) refers to the visible energy in the detector, calculated as the sum of all contained energy losses along the best-fit hypothesis. The total deposited energy serves as a lower limit for neutrino energy and is used as a direct observable in the likelihood fit (see Section ??). Not all energy is deposited in the detector; some may be carried away by secondary neutrinos from tau decays or by muons that leave the detector, while some energy may remain invisible during hadronic showers. Therefore, the sensitivity of total deposited energy to primary neutrino energy varies by event morphology. In single and double cascade topologies, the initial energies of electron and tau neutrinos can be constrained more accurately than those of muon neutrinos, as muon usually leaves the detector and also the energy losses are stochastic, making the proxy weaker.

The Reconstructed length (L_{reco}), represents the distance between two cascades in double cascade events, is a critical observable for tau-neutrino interactions.

The energy asymmetry (E_A) measures the distribution of deposited energy between the two cascades in a double cascade event. It is defined as,

$$E_A = \frac{E_1 - E_2}{E_1 + E_2} \quad (1.6)$$

[13]: Usner (2018), *Search for Astrophysical Tau-Neutrinos in Six Years of High-Energy Starting Events in the IceCube Detector*

9: 4 length seeds shifted 3 times, giving total of 12 seeds

[30]: Stachurska (2020), *Astrophysical Tau Neutrinos in IceCube*

Quality Criteria for `taupede` fit

The final-best fit of `taupede` is accepted only if all the following criteria are satisfied:

- `taupede` Fit is converged
- Energies of both of the fitted cascades $E_1, E_2 \geq 1 \text{ TeV}$
- Both cascades are *softly* contained (vertex $\leq 50 \text{ m}$ outside detector)
- Opening angle between `taupede` and `mumillipede` fit $\leq 30^\circ$

10: If any of the quality checks are failed, the event is assigned track or cascade morphology depending on which of the fit's likelihood is higher.

Direction definitions in IceCube

The zenith angle (θ) gives the direction of particle origin with respect to the vertical axis that points towards the surface of the ice and upward from the South Pole.

A zenith angle of 0° indicates a particle moving directly downward in the detector, 90° corresponds to horizontal propagation, and 180° signifies a particle moving directly upward.

The azimuth angle (ϕ) gives the direction of particle origin with respect to the horizontal x-axis of the IceCube coordinate system (see Section ??)



Figure 1.7: A sketch of energy asymmetry, it is a measure of the relative distribution of total deposited energy between the two cascades, as defined in 1.6. Sketch is adapted from [13].

11: since there is no second energy deposition technically, $E_2 = 0$ for a true single cascade

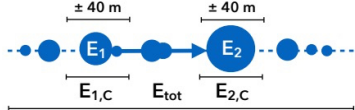


Figure 1.8: A sketch of Energy Confinement, it is a measure of how confined are reconstructed energy depositions E_1 and E_2 are within their reconstructed vertices. The confinement, as shown in the sketch is checked within 40 m of the vertices. Sketch is adapted from [13].

classification Criteria Based on Reconstructed Quantities

After meeting Quality requirements, an event is classified as,
a track if $E_C < 0.99$
a single cascade if $E_C \geq 0.99$ and $(E_A < -0.98 \text{ or } E_A > 0.3 \text{ or } L_{\text{reco}} < 10)$
a double cascade if $E_C \geq 0.99$ and $-0.98 \leq E_A \leq 0.3$ and $L_{\text{reco}} \geq 10$

where E_1 and E_2 are reconstructed energies of the first and the second cascades. A *true*[†] single cascade has an energy asymmetry of 1¹¹, while a double cascade can have any value between -1 and 1, depending on the kinematics of the neutrino interaction. This variable hence, is an excellent estimator to distinguish between a single and a double cascade.

The energy confinement (E_C) measures how much of the total energy is localized near the cascade vertices. It uses the two cascade vertices fitted by taupede and deconvolves the energy depositions within 40 m of each of them. It is defined as,

$$E_C = \frac{E_{1,c} + E_{2,c}}{E_{\text{tot}}} \quad (1.7)$$

where, $E_{1,c}$ and $E_{2,c}$ are the deconvolved energy depositions within 40 m distance of first and second cascades respectively and E_{tot} is the total deposited energy as defined above. Note that from Equation 1.7, $E_C = 1$ (with $E_{1,c} + E_{2,c} = E_1 + E_2 = E_{\text{tot}}$) for a $\nu\bar{\nu}$ induced double cascade, as opposed to tracks which have energy depositions outside the region around the double cascade vertices. It is therefore a suitable estimator to separate single cascades and double cascades from tracks,

The classification chain uses several variables to categorize events into three morphologies. If the taupede fit meets all the quality criteria, a series of selection cuts is applied. If the event passes all these cuts, it is classified as a double cascade, as illustrated in Figure 1.9. Initially, only high-energy starting events (HESE) with a total energy $E_{\text{tot}} \geq 60 \text{ TeV}$ are selected to almost entirely eliminate atmospheric muons. If the quality criteria fail based on the likelihood value, the event is assigned either a single cascade or track morphology. The next step ensures that the reconstructed length $L_{\text{reco}} \geq 10 \text{ m}$. This condition is necessary because while a double cascade with a length below this threshold could be genuine, the resolution of the reconstruction algorithm does not allow for a definitive classification. Therefore, if the length is below 10 meters, the event is classified as a single cascade. As stated before, cuts on E_A and E_C are applied afterward to further filter out single cascades and tracks from the double cascade samples, respectively. Notably, after the quality cut, it is assumed that the event is a double cascade until any of the selection criteria based on reconstructed properties fail.

A noteworthy point is that none of the events in the HESE sample, with $E_{\text{tot}} \geq 60 \text{ TeV}$, are discarded. They are only separated into three sub-samples based on their tagged morphology. All the cuts and selection criteria introduced so far were determined by evaluating the signal-to-background ratio in the distributions of these variables [13]. The cut values were not strictly enforced to allow for some background contribution in the final sample. The rationale behind this selection is that the analysis performed using these three sub-samples is a forward-folding fit (see Section ??). This analysis employs Monte Carlo PDFs that utilize the shapes of signal and background distributions to compare them with data events. Therefore, it is essential to have a sufficient amount of background simulation present in the sample.

[13]: Usner (2018), *Search for Astrophysical Tau-Neutrinos in Six Years of High-Energy Starting Events in the IceCube Detector*

[†] *true* event morphologies are assigned by going through produced charged particles at Secondary Charged Particle Propagation stage of the simulation chain (see Section 1.1.1). Looking at the type of particles, their energy depositions and positions within the detector volume, a morphology is assigned to the event.

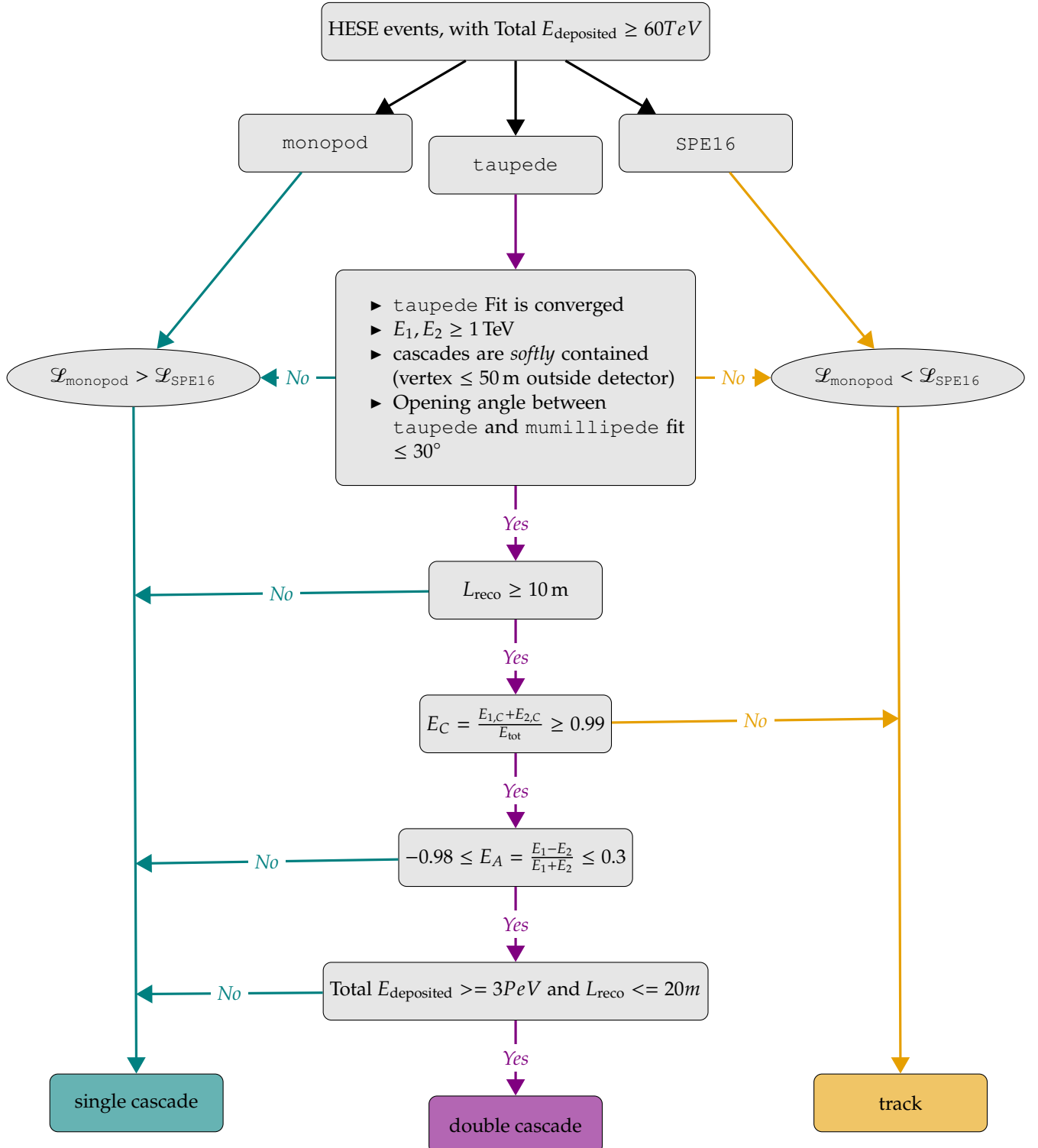


Figure 1.9: The event classification scheme for the Ternary PID. The first level evaluates reconstruction quality; if the criteria are not met, events are classified as single cascades or tracks based on the likelihood values L_{monopod} and L_{SPE16} . The second level considers the reconstructed length, using a threshold below which distinct vertices of double cascades appear as a single cascade. The third and fourth levels focus on energy confinement and energy asymmetry, respectively. The last level is added to improve purity of the double cascade sample at high energies where misclassification is prominent due to glashow events.

So far, all the explained sample selection and Ternary classification has been taken (with updates in simulations and reocnstruction tables) as it was done and used in previous iterations of HESE flavour measurements

[13]: Usner (2018), *Search for Astrophysical Tau-Neutrinos in Six Years of High-Energy Starting Events in the IceCube Detector*
[30]: Stachurska (2020), *Astrophysical Tau Neutrinos in IceCube*

The Sampling correction here refers to changing the weight of the simulated neutrino, and not changing the HESE sample itself. The weight of a simulated neutrino, as discussed in Section 1.1 takes into account various probabilities, such as interaction type, propagation through earth etc. Most of these probabilities are derived from underlying theoretical models of particle interactions [31]. The correction applied here refers to updates in calculations of these models that affects shape of the underlying cross-section and kinematics of the interactions, that may result in difference in reconstructed variable distributions.

[32]: Glashow (1960), *Resonant Scattering of Antineutrinos*

[13, 30]. For the analysis presented in this thesis, some changes were made both in **sampling** and classification schemes that are discussed in the following subsections.

1.4.1 Reclassification of PeV Double Cascades

The Double Cascade sample is crucial for flavor measurement, necessitating a more comprehensive assessment. Using the ternary classification described, the **Flavour Purity** of this sample can be determined. Flavour purity is defined as the fraction of a *desired* neutrino flavor within a given morphology sample. This concept is illustrated in Figure 1.10, which displays the reconstructed energy distribution of the Double Cascade sample for each neutrino flavor. Ideally, one would want that each bin in this plot reflects a 100% contribution from the ν_τ flavor. While it does not achieve 100%, it is evident that the Double Cascade sample is predominantly made up of ν_τ events across the energy range. However, a rapid decrease in purity is observed at high energies (around 6 PeV), where the sample becomes dominated by ν_e events (see the left panel of Figure 1.10). This shift is due to the Glashow resonance of $\bar{\nu}_e$, which significantly influences the cross-section of neutrino interactions at these energies [32]. These events are categorized as Double Cascades because of their high energy deposition over a short distance, but they are misclassified as single cascades.

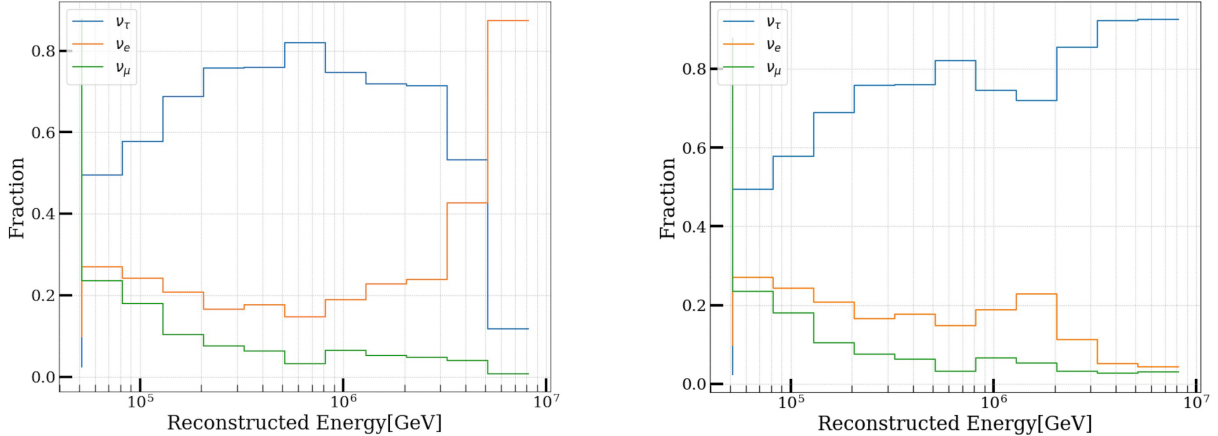


Figure 1.10: Fraction of flavor content per bin in double cascade events. The left panel shows the distribution without the criteria of Total $E_{\text{deposited}} \geq 3 \text{ PeV}$ and $L_{\text{reco}} \leq 20 \text{ m}$, indicating *purity contamination* at high energies from $\bar{\nu}_e$ Glashow events. The right panel presents the distribution after reclassifying double cascades as single cascades under these conditions.

To address this, a **reclassification** mask was introduced at the end of the classification chain outlined in Figure 1.9. If an event is classified as a Double Cascade with a reconstructed energy of $E_{\text{tot}} \geq 3 \text{ PeV}$ and a reconstructed length $L_{\text{reco}} \leq 20 \text{ m}$, it is reclassified as a single cascade. These thresholds were chosen based on the purity distribution to maximize the signal-to-background ratio, even at these energies. The distribution before and after applying this mask is shown in the right panel of Figure 1.10. As anticipated, the lower energy distributions remain nearly identical, while purity is restored at higher energies. It is important to note that the fraction of ν_μ remains unchanged in both figures, due to the involvement of only electron neutrinos—technically electron anti-neutrinos—in Glashow interactions, which contribute to

the purity contamination. Since this is merely a reclassification, the total High-Energy Starting Event (HESE) sample remains unchanged.

1.4.2 Tau Polarisation

As discussed in ??, ν_τ -CC interaction always produces a tau lepton, which has various decay modes. The tau lepton produced in this interaction is polarised, which can significantly alter the kinematics of the tau decay [33, 34]. Whether the decay mode is leptonic or hadronic, the fraction of energy going to the decay products ($\frac{E_{\text{hadrons/leptons}}}{E_\tau}$), is affected if non-zero tau Polarisation is not taken into account. The PRPOSAL software used in simulation presented in this thesis, to simulate secondary charge particle production, propagation and energy losses does not take into account this factor. That is, the Taus produced in a ν_τ -CC interaction is assumed to be produced with no polarisation. Since, the signature which is used for identification of this analysis relies on both, the neutrino interaction cascade and tau decay cascade, not taking in account this correction can lead to an *incomplete* simulation of energy loss profiles. Mainly the energy reconstruction of the second decay cascade, may get affected, which can further alter the Energy asymmetry (E_A) of the event, which is used as a selection variable in Ternary Classifier (see Figure 1.9).

The idea is to test the impact of tau polarisation on analysis variables by reweighting the monte carlo events. The calculations provided in [33], are used to get theoretical fractional energy loss of the electromagnetic equivalent visible energy losses, for both polarised and unpolarised states. The ratio of this is multiplied with the simulated fractional energy (which assumed unpolarised taus), to get a new reweighting factor. The change introduced minor difference in the overall observable distributions, hence this was left as a weight correction only and no further analytical checks were performed.

1.4.3 Glashow Cross-Section correction

The resonance enhancement of $\bar{\nu}_e e^-$ scattering at an energy of approximately 6.3 PeV, known as the *Glashow resonance*, was discussed in Section ?? . The cross-section for this process at this energy is significantly larger—about two orders of magnitude greater—than that of Deep Inelastic Scattering (DIS). Since this energy range is relevant to the thesis presented in this work, it is crucial to consider second-order QCD corrections, which can significantly alter the Glashow cross-section [35].

The corrections applied to the cross-section, as described in [35], include *Initial State Radiation (ISR)* [36, 37] and the *Doppler broadening effect* [38]. ISR becomes more prominent when the center of mass (COM) energy of the system is much higher than the mass of the initial lepton—since W^- is substantially more massive than e^- , this leads to an enhancement factor of approximately $\frac{M_W}{m_e} \sim 12$ in radiation, on top of contributions from the fine structure constant (α). This results in collinear photon emission. Doppler broadening occurs due to the motion of atomic electrons, where the typical velocity of the electron is assumed to be close to the speed of light. This motion causes the COM energy to shift by a factor of

[33]: Garg et al. (2023), *Neutrino propagation in the Earth and emerging charged leptons with nuPyProp*

[34]: Argüelles et al. (2022), *Tau depolarization at very high energies for neutrino telescopes*

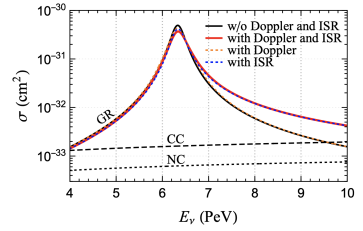


Figure 1.11: The cross section for the Glashow resonance process $\nu_e + e^- \rightarrow W^- \rightarrow X$ is shown with and without initial state radiation and Doppler broadening. The black curve represents the cross section without these effects, the blue dotted curve includes initial state radiation, the orange dotted curve shows Doppler broadening, and the red curve combines both effects. Figure taken from [35].

[35]: Huang et al. (2023), *Inferring astrophysical neutrino sources from the Glashow resonance*

[36]: Garcia et al. (2020), *Complete predictions for high-energy neutrino propagation in matter*

[37]: Gauld (2019), *Precise predictions for multi-TeV and PeV energy neutrino scattering rates*

[38]: Loewy et al. (2014), *The Effect of Doppler Broadening on the 6.3 PeV W^- Resonance in $\bar{\nu}_e e^-$ Collisions*

[27]: Aartsen et al. (2014), *Energy Reconstruction Methods in the IceCube Neutrino Telescope*

$(1 - \beta \cos \theta)$, where θ is the angle between the electron's velocity (β) and the incoming neutrino in the lab frame [38].

The combined results of these effects, based on calculations from [35], were used to adjust the *total weight* of neutrinos. As noted in [35], these effects are smoothed out by the energy resolution of IceCube [27], and the impact of this reweighting on energy distributions and sensitivity was negligible. Nevertheless, the reweighting was retained, similar to the correction for Tau polarization.

1.5 Influence of South Pole Ice properties on Double Cascades Reconstruction

[39]: Chirkin et al. (2013), *Evidence of optical anisotropy of the South Pole ice*

12: Technically it coincides within 1° of the ice flow axis, hence this axis was given a special name, *the anisotropy axis*. The axis along which scattering is reduced is called *the major anisotropy axis* and the one perpendicular to it where scattering is enhanced is known as *the minor anisotropy axis*.

While the SpiceBfr model agrees much better with the data, compared to Spice-3.2.1, it is important to note that on the analysis level, where one uses reconstruction algorithms based on all of the pulse information from the DOMs, the ever so significant effects on charge and time level may get smeared off from overall observable distributions. Going from Spice-mie to Spice-Lea was a breakthrough as the former did not consider this anisotropic behavior of photon propagation. But going from Spice-3.2.1 to Spice-Bfr was more in the direction of inherent modeling of the ice (crystal) property, to explain the anisotropy, while Spice-3.2.1 and Spice-Lea used an approximated solution in the form of effectively mimicking an anisotropic scattering of photons.

[13]: Usner (2018), *Search for Astrophysical Tau-Neutrinos in Six Years of High-Energy Starting Events in the IceCube Detector*

13: This icemodel is almost identical to the one used in previous iteration of this analysis [30]

The identification of ν_τ -induced double cascades in the IceCube detector faces significant systematic uncertainties due to the anisotropy of the ice. As discussed in Section ??, the Anisotropy at the south pole ice has been established since 2013 [39]. This phenomenon causes photons to have a directional dependence while scattering, with enhanced scattering occurring perpendicular to the ice flow axis¹² and reduced scattering along it.

Such a direction dependednt scattering pattern can cause a bias in reconstructing specifically a double cascade event using `taupede`, as this algorithm looks for energy depositions around vertices along a given seed direction (see Section 1.4), which can cause bias in length reconstruction. When a single cascade aligns with this major anisotropy axis, reduced scattering can elongate its apparent size, mimicking double cascade characteristics due to altered light timing at the DOMs. Conversely, if a true double cascade aligns with one of the minor anisotropy axes, it may be compressed, increasing the risk of misidentification as a single cascade. Without accounting for anisotropy, true single cascades could be misclassified as double cascades, while genuine double cascades along minor axes might be missed.

Reconstructing these events relies on photo-spline tables introduced in Section 1.3, which provide tabulated light yields for simulated 1 GeV cascades. These cascades are placed in the detector's center at intervals of $\Delta z = 20$ m, between depths of -600 to 600 m and zenith angles from 0° to 180° . The initial model primarily considers the ice layer's depth and zenith angle for light propagation, but an additional azimuthal dimension was necessary to account for anisotropy. A key advancement was the development of **the effective distance spline tables**, which adjusted for anisotropy by using an isotropic-ice-equivalent position instead of position of the DOMs to look-up for the light yield, which resulted in a significant enhancing of length reconstruction accuracy [13].

Recent developments in icemodel studies have revealed that the directional behavior of light in ice, is due to its molecular structure, a phenomenon known as *birefringence* as already introduced in Section ???. This is now incorporated into the new ice model, called as, **SpiceBfr**. However, during the development stage of the analysis presented in this thesis, the only large-scale Monte Carlo simulations available was the one produced using an earlier icemodel, **Spice-3.2.1**¹³. Naturally, the question

Table 1.1: The four comparison scenarios that were analyzed. The First icemodel in the name always refers to the one used in simulation (second column) and the second refers to the one used in reconstruction (reconstruction). Last column points to corresponding figures.

Name	Simulation Icemodel	Reconstruction Icemodel	
Spice-3.2.1-Spice-3.2.1	Spice-3.2.1	Spice-3.2.1	Figure 1.12a
Spice-3.2.1-SpiceBfr	Spice-3.2.1	SpiceBfr	Figure 1.12b
SpiceBfr-Spice-3.2.1	SpiceBfr	Spice-3.2.1	Figure 1.12c
SpiceBfr-SpiceBfr	SpiceBfr	SpiceBfr	Figure 1.12d

arises, if SpiceBfr can further improve reconstruction (or discover any previously unknown biases), hence a comparison was needed.

Such a check between Spice-3.2.1 and SpiceBfr was feasible since the spline tables for SpiceBfr were already available. To facilitate cross-comparison, a small statistics (one-third of the full available statistics) simulation set was produced using SpiceBfr. The successfully identified true double cascades are considered, and median length bias ($L_{\text{Reco}} - L_{\text{true}}$) is calculated per azimuth bin (see Figure 1.12). An effective reconstruction algorithm should show no bias (i.e. the difference in length should be zero), unless unaccounted asymmetries exist.

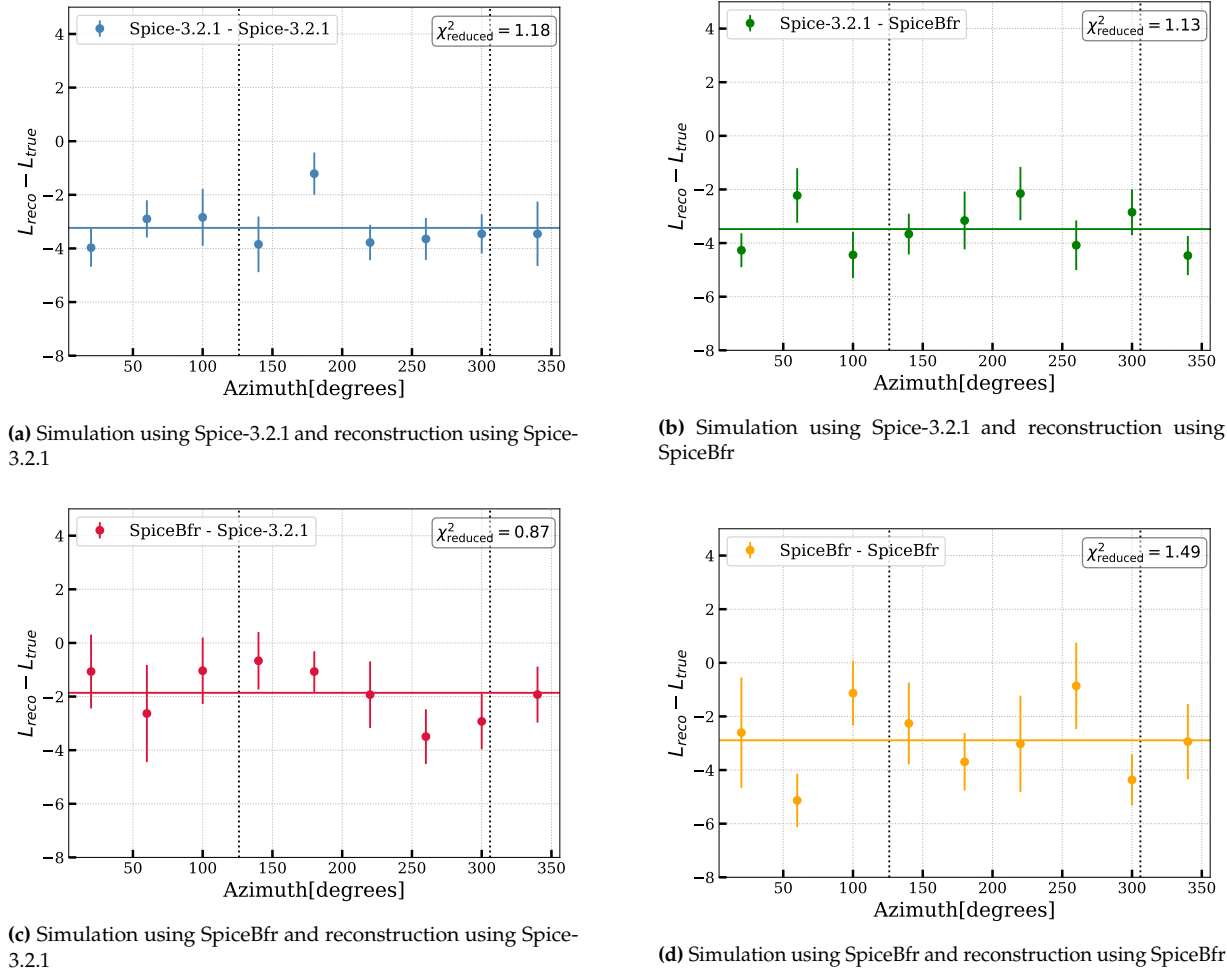


Figure 1.12: Length Bias of true double cascades, classified as double cascades, as function of Azimuth angle. Vertical lines shows the direction of the major anisotropy axis. Caption below each figures shows which combination of icemodel is used in simulation and reconstruction respectively. Each figure also shows reduced value of χ^2 calculated by fitting the showed horizontal line, see text for details.

Since all cases involve either the effective distance correction or an inherent anisotropy parametrization (via birefringence), minimal bias was expected along the major anisotropy axis. As shown in the results, only minor structures were observed, and none were deemed statistically significant, particularly along the anisotropy axis. To probe further, a χ^2 goodness-of-fit (gof) test was performed to fit a horizontal line, with the reduced χ^2 calculated for each of the four cases (values indicated on all figures). The results indicated that all four combinations fit well to a horizontal line, signifying no significant biases were present. However, the plots corresponding to the simulation produced using SpiceBfr (both reconstructed with SpiceBfr (Figure 1.12d) and Spice-3.2.1 Figure 1.12c) showed signs of over/underfitting, likely due to the low statistics of the generated SpiceBfr simulation set.

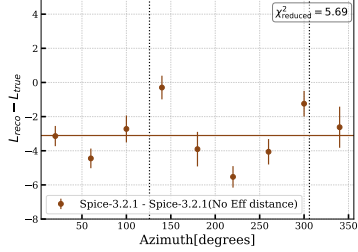


Figure 1.13: Simulation using Spice-3.2.1 and reconstruction using Spice-3.2.1 but no effective distance. See caption of Figure 1.12 for details.

This observed lack of obias aligns with expectations, as Spice-3.2.1 effectively handles anisotropy through the effective distance parameterization. The final step thus, was to verifying if the lack of bias was truly due to the effective distance splines. In Figure 1.13, a distribution is shown where events are simulated using Spice-3.2.1 but reconstructed without the effective distance correction. The resulting reduced χ^2 of 5.69 indicates a poor fit, and a clear bias is visible along the anisotropy axis, as was observed in [13]. This conclusively demonstrates that both Spice-3.2.1 and SpiceBfr, both with appropriate efftive distance corrections are well-suited for analyzing ν_τ -induced double cascades in the presence of ice anisotropy.

Since the SpiceBfr model represents the best current understanding of South Pole ice, the decision was made to proceed with simulations using Spice-3.2.1, reconstructed with the SpiceBfr model. This choice is further supported by the reduced χ^2 values across the four cases, where the combination of Spice-3.2.1 simulation and SpiceBfr reconstruction produced the value closest to 1, indicating the most accurate fit. Consequently, the analysis continued with this combination, ensuring the best possible handling of ice anisotropy in the event reconstruction.

Given that the SpiceBfr model represents the best current understanding of the South Pole ice, the decision was made **to proceed with Spice-3.2.1 simulations reconstructed using the SpiceBfr model**. This approach is further supported by the reduced χ^2 values across the four cases, with the Spice-3.2.1 simulation and SpiceBfr reconstruction yielding the value closest to 1, indicating the most accurate fit. Hence, from here-on, it is to be

Sensitivity of IceCube-Gen2 to measure flavour composition of Astrophysical Neutrinos

2

Siginificant portion of this thesis work was dedicated to assess IceCube Gen2's sensitivity to measure the flavour composition of the astrophysical neutrinos. The detector will be introduced in the following sections, along with the simulations and software framework used to produce the results.

2.1 IceCube Gen2

IceCube-Gen2 is a proposed next generation of neutrino detector, designed to observe the neutrino sky within a wide energy range, from TeV to EeV [40]. Its sensitivity is expected to be at least five times better than IceCube, enabling the observation of individual sources. The instrument layout is designed to detect about ten times more neutrinos annually as compared to IceCube. This increased capability will facilitate in-depth studies of the distribution of neutrinos across the sky, energy spectrum, and flavour composition, as well as beyond-the-Standard-Mode.

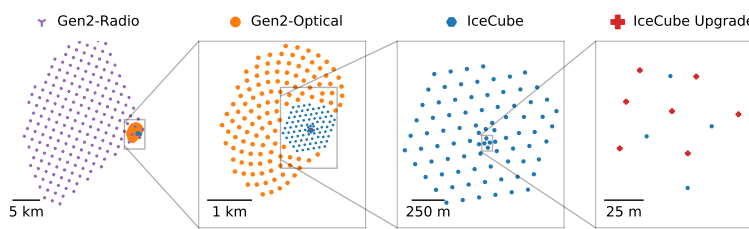


Figure 2.1 illustrates a top view of the IceCube-Gen2 facility, showcasing its various components using optimized technologies for the targeted energy ranges.

The *IceCube Upgrade* will start deployment this season (2024-2025 austral summer). Its goal is to lower the detection threshold for neutrinos to 1 GeV (In-line with its predecessor, *DeepCore* in current IceCube)[41]. This improvement will advance oscillation measurements, dark matter searches, and studies of physics beyond the Standard Model. The IceCube Upgrade project will also deploy 693 new multi-PMT detector modules on 7 new strings as shown in right-most panel of Figure 2.1, providing an opportunity to test the optical sensor technology for the IceCube-Gen2 observatory.

The *Surface Array* of IceCube-Gen2 is a setup of scintillator detector arrays on the surface of the South Pole, that measures the electromagnetic shower component and low-energy muons, while the optical array detects \geq TeV muons from the same air shower [42]. Planned to be used similarly as *IceTop* of IceCube (see Section ??), the stations shall be placed on top of the additional *in-ice* strings of optical array. It can also be used as *surface veto* to reduce the

2.1	IceCube Gen2	19
2.2	Simulation	20
2.2.1	Isotropic Sensor	21
2.2.2	Event Selection	22
2.3	Analysis tool: <code>toise</code> . .	24
2.4	Result of Flavour Sensitivity Measurements	25

[40]: Aartsen et al. (2021), *IceCube-Gen2: the window to the extreme Universe*

Figure 2.1: Figure depicts the proposed IceCube-Gen2 Neutrino Observatory facility at the South Pole. It includes (from left to right) (i) a radio array with 200 stations, (ii) 120 new *in-ice* strings, spaced 240 m apart (shown as orange points), as an expansion of (iii) current optical array, (iv) 7 strings of IceCube upgrade, to be deployed soon within current *in-ice* DeepCore volume. Figure taken from [40]

[41]: Ishihara (2021), *The IceCube Upgrade - Design and Science Goals*

[42]: IceCube Collaboration et al. (2024), *IceCube-Gen2 Surface Array: Science Case and Plans*



Figure 2.2: The designs of the IceCube-Gen2 optical sensors, DOM-16(second) and DOM-18 (third) with their base designs, to be used in the IceCube Upgrade sensors, are the mDOM on the left and D-Egg on the right [46]

[43]: Askar'yan (1961), *Excess negative charge of an electron-photon shower and its coherent radio emission*

[44]: Meyers et al. (2021), *Radio Detection of EeV Neutrinos in Dielectric Media using the Askaryan Effect* for Babies*

[45]: Aguilar et al. (2019), *The Next-Generation Radio Neutrino Observatory – Multi-Messenger Neutrino Astrophysics at Extreme Energies*

[40]: Aartsen et al. (2021), *IceCube-Gen2: the window to the extreme Universe*

background of atmospheric muons in samples of astrophysical neutrinos from the southern sky.

The Radio Array aims to discover and characterize the high-energy neutrino flux above 10 PeV. It detects nanosecond-scale radio emissions from ultra-high-energy particle showers using the Askaryan effect [43, 44]. This technique is sensitive to energies above a few PeV and complements the energy range of the optical array by capturing radio emissions from neutral and charged-current interactions, as well as energy losses of secondary leptons. The initial stations of the Radio Neutrino Observatory in Greenland, will serve as a R&D tool for the Radio component of IceCube Gen2 [45].

The Optical Array The optical array will be expanded with the addition of 120 new strings to the existing IceCube strings. The strings will be arranged in what is referred to as "sunflower geometry," with an average horizontal spacing of 240 meters. The shape of the array and spacing between the strings will be determined through dedicated geometry optimization studies. Each string will contain 80 modules, resulting in a total of 9600 new modules. These modules will be placed between 1325 meters and 2575 meters below the surface, with a vertical spacing of 16 meters. This configuration will create an instrumented geometric volume of 7.9 cubic kilometers. The modules on the string are expected to collect nearly three times the number of photons gathered by an IceCube digital optical module (DOM) [40].

For the sensitivity study presented in this thesis, only the optical part of the proposed detector was simulated and used.

2.2 Simulation

To perform this sensitivity study, dedicated simulations were carried out. The study aims not only to assess the sensitivity of IceCube-Gen2 for measuring the flavour composition of astrophysical neutrinos but also to evaluate its capabilities for detecting tau neutrino events, which is a crucial component as described in Chapter 1. The simulations were aligned with the mainline IceCube simulations (detailed in Section 1.1.1) to enable direct comparisons. However, necessary modifications were made to account for the new-generation optical sensors to be used in IceCube Gen2 and the sparser geometry.

The following sections will describe the event samples created using these simulations to conduct the sensitivity analysis. First a brief overview of the *simulated* sensor shall be given, where an isotropic sensor was created by assuming a spherical PMT, instead of a more realistic multi-PMT module, which requires considerable amount of time and resources to establish. The rest of the simulation chain remains identical to that explained in Section 1.1.1 for mainline icecube simulations,

particle generation → propagation of secondaries → photon propagation → Detector Simulation

Once the simulation is available, the selection cuts are applied to select only high energy events that start within the detector volume, to mimic the so-called High Energy Starting Event (HESE) described in Section 1.2. A classification of all HESE-like¹ events is then performed using a similar particle identifier described in Section 1.4 to classify these events in three morphologies, **Single Cascade, Double Cascades and Tracks**.

2.2.1 Isotropic Sensor

The choice of optical sensors to be used in the IceCube-Gen2 project depends strongly on how well the reference optical sensors to be deployed in the IceCube upgrade perform.[46]. The designs have been carefully optimized to balance cost-effectiveness, logistical efficiency, and enhanced performance. Figure 2.2 shows both the 16 and 18 PMT modules, which are being considered to use in IceCube Gen2, along with **mDOM** (*multi PMT Digital Optical Module*) [47, 48] and **D-Egg** (*Dual optical sensors in an Ellipsoid Glass for Gen2*) [49] that are to be deployed in ice for IceCube Upgrade.

The maturity of the design, along with extensive in-situ testing using a large number of sensors for the IceCube Upgrade, leads us to consider the mDOM-type sensor as the baseline for evaluating the IceCube Gen2 detector's capabilities in identifying Tau neutrino-induced Double Cascade events. Unlike IceCube's single large 10" PMT, the mDOM consists of 24 smaller 3" PMTs. The key advantages of the mDOM over pDOM [50] are its 2.2 times higher effective photocathode area, omnidirectional sensitivity, and the directional information obtained from the individual "pixels" (the 24 PMTs). Due to the large number of PMTs and their strategic placement within the module sphere, this module offers nearly isotropic angular acceptance, unlike IceCube DOMs with only one downward-facing PMT.

The effective area of the optical modules is the equivalent physical cross-section that would detect all the incident photons from a plane perpendicular to a given direction. As illustrated in Figure 2.3 (Left plot), the mDOM has a nearly constant effective area for collecting photons from all directions, unlike the Gen1 DOMs (pDOMs) which have a downward-facing PMT. As a result, the effective area for pDOMs increases as the arrival direction shifts from 180 degrees ("down-going" in the IceCube coordinate system) to 0 degrees ("up-going" in the IceCube coordinate system).

¹: The selection is referred as HESE-like and not exactly HESE as the original selection is sensitive to the detector geometry where outer layer DOMs are used as an active veto as described in Section 1.2. For this sensitivity study, an approximation was made by matching the effective area of sample derived using IceCube-only strings.

[46]: "Abbasi et al. (2023), *The IceCube Gen2 Technical Design Report*

[47]: Classen et al. (2017), *The mDOM - A multi-PMT digital optical module for the IceCube-Gen2 neutrino telescope*

[48]: Classen et al. (2019), *A multi-PMT Optical Module for the IceCube Upgrade*

[49]: Abbasi et al. (2023), *D-Egg: a dual PMT optical module for IceCube*

pDOM

pDOM stands for PINGU Digital Optical Module. It was first coined for an R&D upgrade of IceCube Deep-Core called PINGU (The Precision IceCube Next Generation Upgrade) [50].

[50]: "Aartsen et al. (2014), *Letter of Intent: The Precision IceCube Next Generation Upgrade (PINGU)*

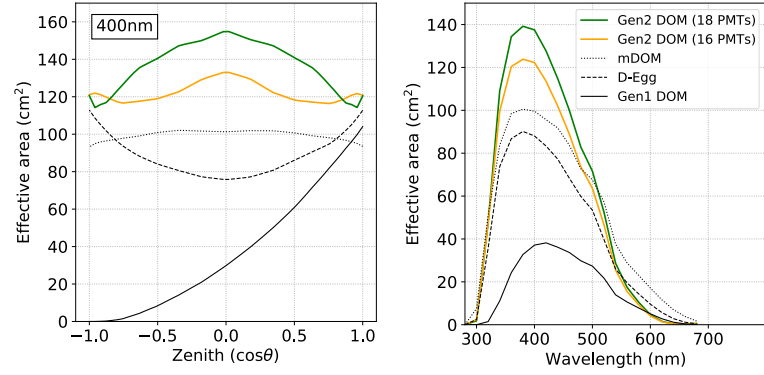


Figure 2.3: The effective area is compared for IceCube-Gen2 DOM candidates, 16, and 18 PMT models, in relation to IceCube-Gen1 DOM (pDOM), D-Egg, and mDOM, as functions of zenith angle (left) and wavelength averaged over solid angle (right). Figure taken from [46]

[51]: Omeliukh (2021), *Optimization of the optical array geometry for IceCube-Gen2*

However, current simulation methods used in IceCube (see Section 1.1) do not yet provide a detailed simulation of a multi-PMT module, so a simulated sensor called *iso-pDOM* (isotropic-pDOM) was developed [51]. This sensor can be thought of as a ‘spherical PMT’ encased in a glass vessel similar to an IceCube DOM but with 2.2 times higher quantum efficiency, capable of capturing photons arriving from all the directions (see Figure 2.4). The sphere was simulated by assuming an upward-facing PMT along with a downward one and combining the results while maintaining the same area under the curves at all wavelengths. The resultant iso-pDOM has an effective area very similar to that of an mDOM.

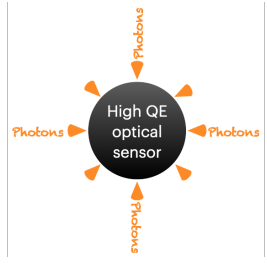


Figure 2.4: Conceptual representation of Simulated sensor with isotropic angular acceptance (iso-pDOM)

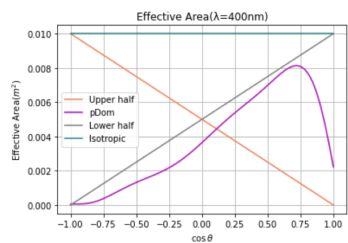


Figure 2.5: Results of simulating a sensor that *mimics* the behaviour of a typical mDOM. The blue line shows changed effective area of the so-called *isoPDOM*, achieved by combining acceptance curves of pDOMs having a PMT in "upper" (orange) and "lower" (grey) halves of the DOM respectively

2: IC86 stands for the current IceCube detector volume, made up of 86 strings containing Digital Optical Modules (DOM).

2.2.2 Event Selection

Monte Carlo events were produced using isoPDOM for all three flavours of primary neutrinos with energies ranging from 100 TeV to 50 PeV. The simulation chain is identical to that described in Section 1.1. It is important to note that since the IceCube in-ice array is inherently part of the proposed Gen2 detector, all simulated events still include information (collected charge) collected by IceCube DOMs from the IC86² configuration. Additionally, during the Detector Simulation stage of the simulation chain (see Section 1.1), where PMT responses, noise, etc., are added, responses are incorporated separately for IceCube DOMs and isoPDOMs. If an event passes all the basic triggers, two separate triggers are stored depending on the event location: IC86 and ICGen2. By default, ICGen2 has a combined response of both detector configurations, while IC86 only contains current IceCube volume events. This feature is crucial as it facilitates direct comparison of events produced with IceCube simulations for IceCube-only analyses.

A fundamental aspect of flavour measurement studies is the ability to identify the flavour of the neutrino involved in an interaction. This identification is possible due to the distinct by-products produced by different neutrino interactions, which result in unique light deposition patterns, or “morphologies” as described in Section ???. These patterns, illustrated in Figure ???, allow us to reconstruct the events by analyzing the pattern of photon detections in the detector. By doing so, the flavour of the original interacting neutrino can be determined.

To utilize the same particle identifier used in the analysis presented

in Chapter ?? for this sensitivity study, a dedicated event selection process for high-energy starting events (HESE) [19] was implemented. However, since the outer-layer detector veto is specific to the detector geometry and the characteristics of the DOM pulses—which is still under development for the IceCube-Gen2 simulation chain-starting events were selected by examining the interaction vertex of the primary neutrino. This interaction vertex was further refined by considering the deposited charge (measured in single photoelectrons) and calculating the charge-weighted mean positions. This charge information is crucial for applying a HESE-like charge cut. Unlike the 6000 photoelectrons threshold used previously, the threshold for this analysis was set at 2000 photoelectrons. The lower threshold is due to the higher quantum efficiency and isotropic sensitivity of the new sensors, which enhance the detection capability for high-energy events. All the approximations made were in parallel checked for IC86 configuration to reproduce Monte Carlo PDFs within statistical errors to the ones presented in analysis chapter.

Moreover, to appropriately weight the simulated events and account for the probability of an atmospheric neutrino being rejected by an accompanying muon triggering the veto, a dedicated calculation similar to the one used in the HESE-7.5 analysis [19] was used. Additionally, the reconstructed energy cut, initially set at 60 TeV, was adjusted to 100 TeV. This adjustment was based on the signal-to-background probability density functions (see Figure 2.6) to ensure a similar signal-to-background ratio (2:1) as achieved in the HESE-7.5 analysis [21] and the HESE-12 analysis, presented in Chapter ?? and Chapter ???. A peculiar observation while looking at Monte Carlo PDFs shown in Figure 2.6 compared to those shown in Figure ?? can be seen due to limited number of produced Monte Carlo for this study. Although, even with low statistics, more population along the LvsE diagonal is clearly visible on the left panel showing signal Double Cascade events.

After applying all the necessary filters, the final sample includes starting events with a reconstructed deposit energy of 100 TeV or more and a charge exceeding 2000 PE. These events originate from interactions of all six types of neutrinos (particle and antiparticle versions of 3 flavours) beginning within the simulated IceCube-Gen2 fiducial volume. They are divided into three categories: Tracks, Single Cascades, and Double Cascades.

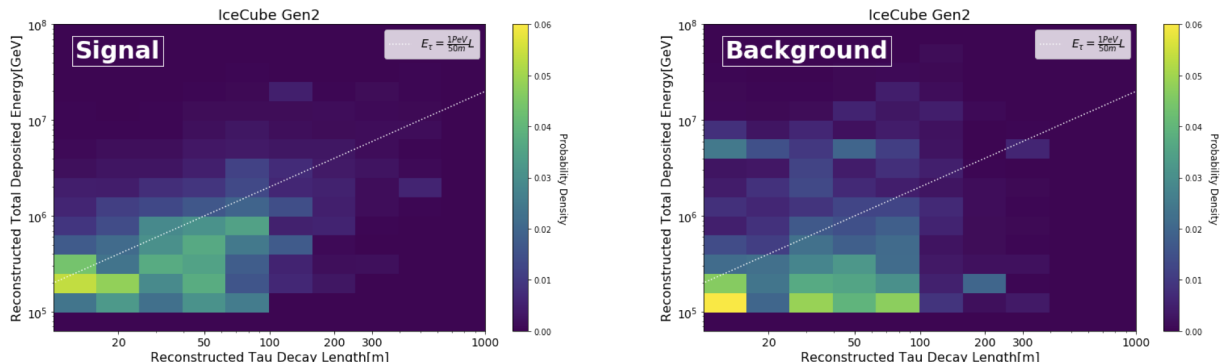


Figure 2.6: 2D Monte Carlo templates, constructed using reconstructed total energy (E_{Tot}) and double cascade length (L_{dc}) for events classified as **double cascades**. The signal (left), representing ν_τ -induced double cascades, shows a clear correlation between L_{dc} and E_{tot} . In contrast, the background (right), consisting of ν_μ and ν_e events, lacks this correlation and clusters at low L_{dc} .

[19]: Abbasi et al. (2021), *IceCube high-energy starting event sample: Description and flux characterization with 7.5 years of data*

[19]: Abbasi et al. (2021), *IceCube high-energy starting event sample: Description and flux characterization with 7.5 years of data*

[21]: Abbasi et al. (2022), *Detection of astrophysical tau neutrino candidates in IceCube*

2.3 Analysis tool : `toise`

Understanding and enhancing the sensitivity of the detector can result in more precise and dependable performance, thus improving the scientific impact of the experiment. The main goal of the sensitivity studies carried out in this work is to optimize the design of the detector in order to be capable of reconstructing tau neutrino events using existing methods, but with a larger detection volume and new generation optical sensors. Additionally, one can also assess the sensitivity of the detector by combining both radio and optical arrays of the proposed detector to investigate flavour measurements in the energy ranges from TeV to EeV [52].

[52]: Coleman et al. (2024), *The flavor composition of ultra-high-energy cosmic neutrinos: measurement forecasts for in-ice radio-based EeV neutrino telescopes*

[53]: Santen et al. (2022), *toise: a framework to describe the performance of high-energy neutrino detectors*

It's impractical to run comprehensive simulations for evolving detector designs due to the large amount of computing power required. The `toise` [53] framework was created to estimate sensitivity using a simplified model of the detector response based on targeted Monte Carlo (MC) simulations. This allows for efficient comparisons of different detector designs without repeating the entire simulation process. `toise` was used for a sensitivity study presented in the next section. This section will provide a brief overview of its workflow. In order to distinguish the influence of design choices on detector performance from the intrinsic restrictions imposed by neutrino interaction physics, the event rate calculation in this framework is conducted through two distinct stages: Neutrino Physics and Detection.

In the Physics stage, the neutrino fluxes at the Earth's surface are converted to the detector's area or volume. This involves using a transfer tensor to model the conversion between the initial neutrino flavour states and the observable final states (muons, hadrons, etc.). In addition, various aspects of neutrino interactions, including neutrino-nucleon cross-sections and different interaction types (neutral current or charged current) are also taken into account. The transfer tensor is subsequently combined with the final-state effective area to establish a neutrino effective area. The effective area $A_{\text{eff}}(E, \theta)$ of the detector is calculated by multiplying the geometric area $A_{\text{geo}}(\theta)$ with an energy and zenith-dependent efficiency $\eta(E, \theta)$:

$$A_{\text{eff}}(E, \theta) = A_{\text{geo}}(\theta) \times \eta(E, \theta) \quad (2.1)$$

For the optical array of the proposed IceCube-Gen2, the geometric area is approximately calculated by placing a convex hull around the instrument's geometric boundary. *The selection efficiency* $\eta(E, \theta)$ characterizes the detector's triggering efficiency and the probability of an event passing a set of analysis criteria. It is defined as *the ratio of events passing these cuts to the number of events generated*. Depending on the type of sensitivity study being performed—such as expected limits, discovery potential, or flavour measurement—additional parameterizations like energy and angular resolutions and classification efficiency are used. For flavour measurement, *the classification efficiency* generates an event classification smearing matrix (Figure 2.8) and is defined as *the fraction of morphology per energy bin for a given neutrino flavour*.

When estimating sensitivities, it is essential to account for backgrounds that may mimic the signal. The framework handles backgrounds by either adding their contributions to the event rate or ignoring regions where they are expected to contribute. For all detectors and science cases, atmospheric neutrino flux is added as a background using the same effective area as for astrophysical neutrinos. Optionally, atmospheric neutrino flux in the downward-going region can be reduced to account for vetoing by accompanying muons from the same air shower. This is done in a similar way to the one described in Section 1.2.

2.4 Result of Flavour Sensitivity Measurements

Using the HESE-like sample, described in Section 2.2.2, a detector response tensor is generated using `toise`. Selection efficiency, detailed in Section 2.3, is a key factor in generating the detector's neutrino effective area. This efficiency is determined using Figure ??, which shows the true deposited energy at which the analysis starts to select events. The plot illustrates the ratio of events passing all selection cuts in Section 2.2.2 to all simulated neutrinos reaching the fiducial volume, per energy bin. The curve is fitted, and the resultant plot shows that neutrinos are selected starting from approximately 200 TeV. This value is used as the selection threshold for events beginning or contained in the fiducial volume.

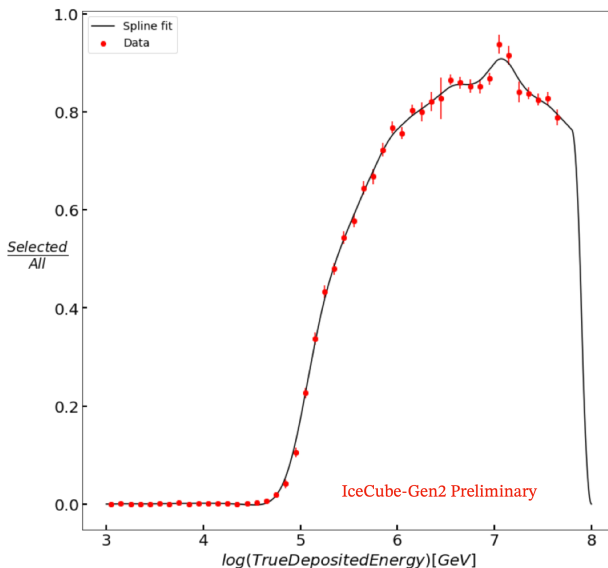


Figure 2.7: Selection Efficiency : Ratio of neutrinos that got classified into a topology to all the neutrinos that interacted in active volume. Data here refers to monte-carlo events per energy bin.

A specific parameterized tensor is used to determine the efficiency of particle identification during flavour measurements. Figure 2.8 shows how well the reconstruction process can identify different types of particles based on their morphologies. In an ideal scenario, events involving charged current interactions with electron neutrinos (ν_e) are classified as single cascades, those involving muon neutrinos (ν_μ) as tracks, and those involving tau neutrinos (ν_τ) as double cascades. The diagonal elements of the plot show how accurate the classifier is, while the off-diagonal elements indicate the fractions of misidentified flavours. The plot shows that as the true deposited energy increases, the number of double cascade events (from ν_τ interactions) initially plateaus and then

decreases. This occurs because at higher energies, the individual energy depositions are further apart (due to correlation of L_{dc} and E_{tot}), making it easier for the reconstruction process to distinguish them. However, at even higher energies, one of the cascades may be partially or completely outside the detector, causing these events to be misclassified as single cascades due to strict containment criteria, as described in Section 1.4. For single cascades involving ν_e , the efficiency decreases at high energies because some DOMs may become saturated, and their data is excluded from the analysis. In contrast, the efficiency for starting tracks remains relatively consistent across the entire energy range.

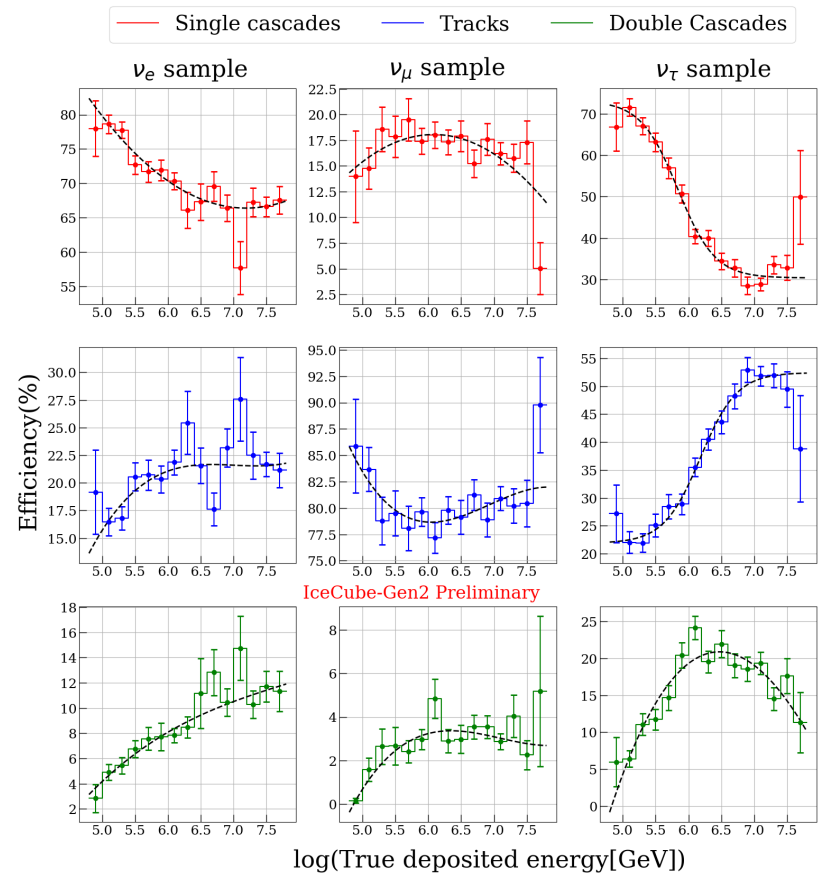


Figure 2.8: Classification Efficiency: Three subplot columns are true neutrino flavours, where each energy bin (true Monte Carlo energy) contains the fraction of topologies, summing to 100%. Diagonal plots show the flavour identification efficiency of the classifier, whereas off-diagonal plots show misidentification fractions.

[54]: Abbasi et al. (2022), *Improved Characterization of the Astrophysical Muon–neutrino Flux with 9.5 Years of IceCube Data*

[55]: Lad et al. (2023), *Summary of IceCube tau neutrino searches and flavor composition measurements of the diffuse astrophysical neutrino flux*

Lastly, a significant advantage of `toise` is its ability to combine different event selections and detector types. The starting event sample from this detailed study can be combined with the efficiencies of other samples, such as through-going tracks sample. In `toise`, these efficiencies are included by limits derived from IceCube analysis [54] to calculate angular resolutions, PSF, etc. The flavour measurement presented here demonstrates the sensitivity of IceCube Gen2 by combining starting events with through-going muons, a method already realized in IceCube [55].

Figure 2.9 shows the projected flavour measurement sensitivity of IceCube-Gen2 with 10 years of data [56]. It is derived by using an asimov dataset [57] assumes equal partition of all flavours, with a diffuse neutrino spectrum following a single power-law with an index of 2.5 and a per-flavour normalization of 2.3 [58]. The confidence intervals are derived by assuming wilks' theorem [59], as for analysis presented in Chapter ???. The figure also illustrates the sensitivity change if a dedicated ν_τ identifier is not included in the starting event sample, resulting in the sample containing only single cascades and tracks, making it impossible to resolve the ν_e and ν_τ fraction degeneracy. The systematic variations arising due to detector are neglected.

[56]: Lad et al. (2023), *Sensitivity of IceCube-Gen2 to measure flavor composition of Astrophysical neutrinos*

[57]: Cowan et al. (2011), *Asymptotic formulae for likelihood-based tests of new physics*

[58]: Aartsen et al. (2015), *A combined maximum-likelihood analysis of the high-energy astrophysical neutrino flux measured with IceCube*

[59]: Wilks (1938), *The Large-Sample Distribution of the Likelihood Ratio for Testing Composite Hypotheses*

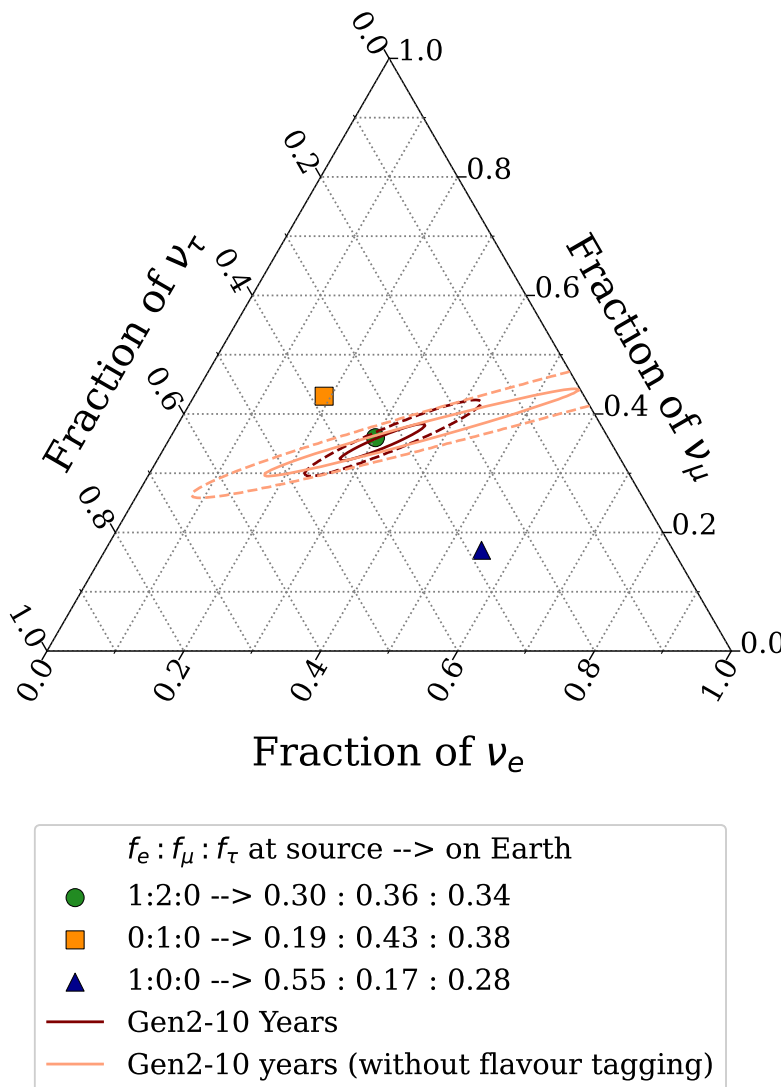


Figure 2.9: Projected sensitivity of IceCube-Gen2 to measure flavour composition of Astrophysical neutrino with 10 years of its lifetime. The maroon line shows sensitivity using the ternary classification scheme and light salmon shade shows sensitivity **without** a dedicated ν_τ identifier. The unresolved degeneracy along ν_e/ν_τ axis is notable due to lack of double cascade classifier. The solid (dashed) lines depict the corresponding 68% (99%) constraints, derived assuming Wilks' theorem.

The sensitivity shown in Figure 2.9 and applies to the entire diffuse neutrino spectrum. With this study, flavour measurement for a given 'slice' of energy was also done to characterize its energy dependence. As described in ???, diffuse neutrino spectrum consists of neutrinos originating from various high-energy sources in all directions. Depending on the environments of the acceleration sites (magnetic fields, accretion disks, dust, etc.), the production ratios of neutrinos at the sites may differ [60]. The most commonly assumed model, is the pion decay scenario (see

[60]: Kashti et al. (2005), *Astrophysical Neutrinos: Flavor Ratios Depend on Energy*

[61]: Winter (2014), *Describing the Observed Cosmic Neutrinos by Interactions of Nuclei with Matter*

[62]: Bustamante et al. (2015), *Theoretically Palatable Flavor Combinations of Astrophysical Neutrinos*

[46]: "Abbasi et al. (2023), *The IceCube Gen2 Technical Design Report*

Section ??). At higher energies, however, due to synchrotron cooling of secondary muons produced in pion decay (see Equation ??) the flavour production at sources changes to a ratio of ($\nu_e : \nu_\mu : \nu_\tau$) from 1:2:0 to 0:1:0 [61]. If such sources begins to dominate the overall flux at high energies, a transition in measured neutrino flavour fluxes can be observed [62]. Figure 2.10 shows IceCube-Gen2's sensitivity to detecting such a flavour transition. The assumed "critical energy" for this mechanism for the study is 2 PeV. This transition is detectable with IceCube-Gen2 due to its extended energy range, enabled by its approximately eightfold increase in volume [46].

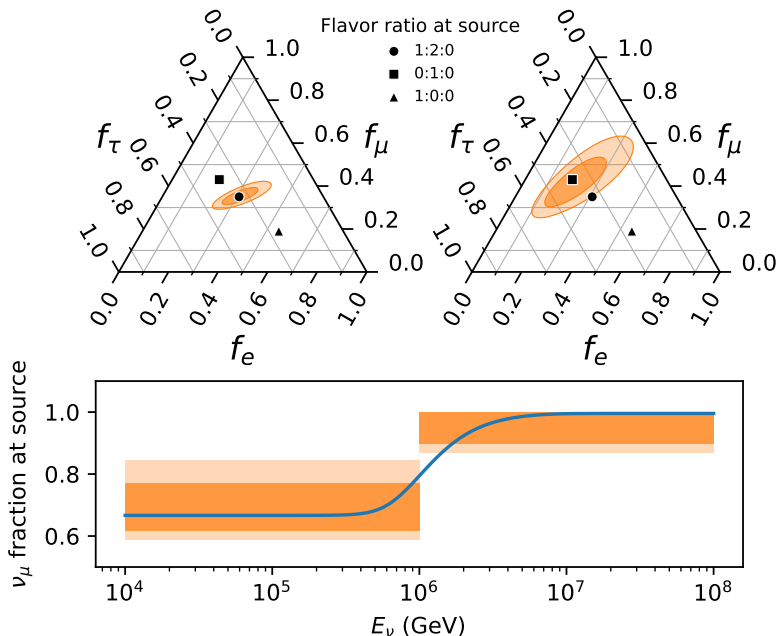


Figure 2.10: The bottom section displays the proportion of ν_μ at the source based on energy, with the assumption that the muon critical energy is 2 PeV. The error bars represent the 68% confidence level limitations on the ν_μ fraction below and above 1 PeV, derived from the observed flavour composition of ν_μ at Earth using IceCube-Gen2 and assuming standard oscillations. In the upper sections, the dark (light) shaded regions depict the corresponding 68% (99%) constraints, without making any assumptions about the mixing matrix.

[52]: Coleman et al. (2024), *The flavor composition of ultra-high-energy cosmic neutrinos: measurement forecasts for in-ice radio-based EeV neutrino telescopes*

[46]: "Abbasi et al. (2023), *The IceCube Gen2 Technical Design Report*

The power of combining different event samples, extension of detector volume along with an isotropic module already shows a significant gain in sensitivity to measure flavour composition of astrophysical neutrinos. Furthermore, the optical component of IceCube Gen2 will also be sensitive to detect a changing flavour composition as a function of neutrino energy, that shall allow us to distinguish population of dominating sources across the spectrum. The study presented above can be further extended by adding the proposed radio component to the sample [52]. As described in Section 2.1, due to the extended radio array IceCube-Gen2 shall be sensitive to measure EeV neutrinos as well [46]. Figure 2.11 shows extension of sensitivity projection shown in Figure 2.10, by adding flavour tagging at higher energies. It shows that at even higher energies, where the diffuse neutrino spectrum is dominated by cosmogenic neutrinos (see Section ??), the measure flavour ratio transitions back to the 1:2:0 scenario at the source [52].

To conclude, IceCube-Gen2's increased volume will improve the detection rate of tau neutrinos, which are identifiable by their unique "double-bang" decay signature. This enhancement in tau neutrino identification, especially above 300 TeV, will provide critical insights into the flavour composition of astrophysical neutrinos, enabling stronger constraints on source physics and the potential to detect new physics beyond the Standard Model. Furthermore, the inclusion of a radio array may extend

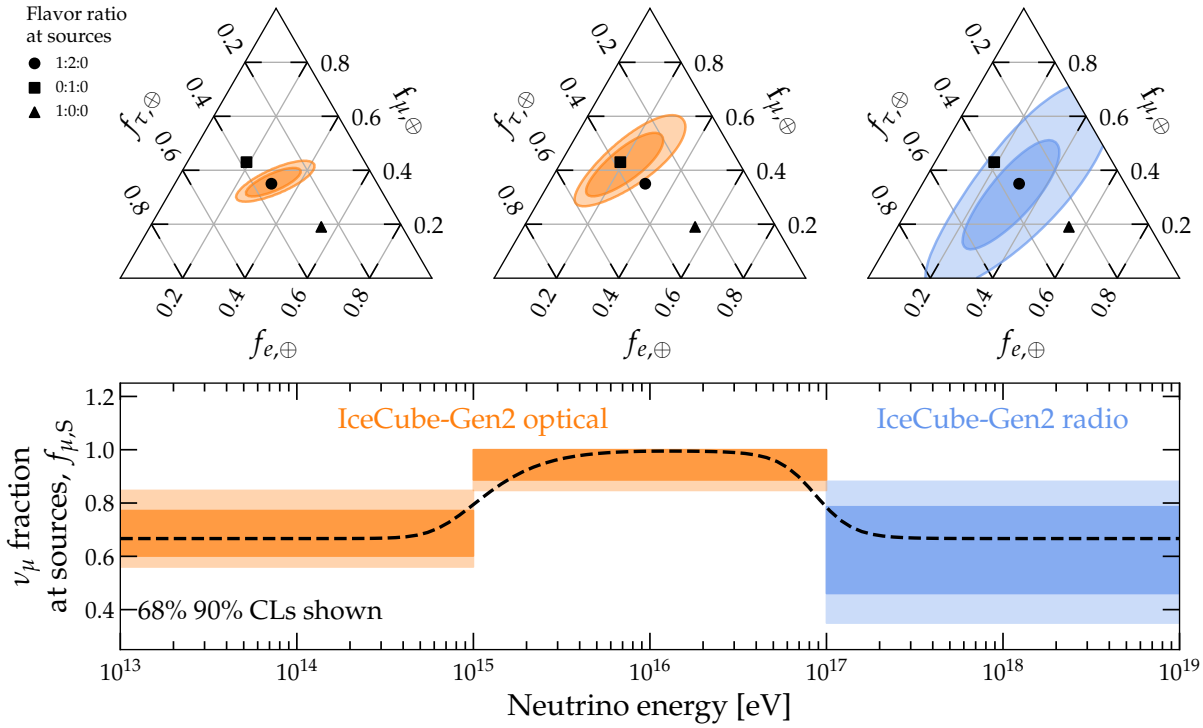


Figure 2.11: A combined sensitivity to measure evolution of the neutrino flavour composition with energy ranges from TeV to EeV range, using both optical and radio components of IceCube Gen2 Detector. Astrophysical neutrino sources are generally expected to be dominated by pion decay at the lowest energies, with a flavour composition of approximately (1:2:0). At intermediate energies, the sources transition to a muon-damped production regime, yielding a flavour ratio of roughly (0:1:0). Finally, at the highest energies, the composition reverts to the pion decay pattern, (1:1:1), as anticipated for cosmogenic neutrino production. The details for layout are similar to that shown in Figure 2.10. The extended figure, taken from [52].

tau neutrino detection capabilities to even higher energies in the EeV range, offering unprecedented precision in exploring the universe's most extreme neutrino sources. The enhanced sensitivity of IceCube-Gen2, achieved through the combination of optical and radio detection methods, will close critical gaps in our understanding of the cosmic neutrino energy spectrum, extending the detection range up to three orders of magnitude higher than current capabilities. This leap in sensitivity will enable the discovery of ultra-high-energy neutrinos, paving the way for transformative progress in both high-energy physics and astrophysics.

APPENDIX

List of Figures

1.1	Light emission pattern of a simulated muon track event, using the direction propagation program CLSIm. The colored lines show individual photon paths through ice, with red indicating earlier and blue indicating later compared to an unscattered photon. Figure taken from [10]	4
1.2	Illustration of the SnowStorm method described in the text. It depicts the contrast between numerous discrete shifts in nuisance parameters (indicated by red squares), each necessitating an entire Monte Carlo set, in comparison to a single SnowStorm Monte Carlo (represented by small blue dots). Figure taken from [16]	5
1.3	The top view (above) and side view (below) display the veto DOMs and the DOMs within the fiducial volume for HESE. DOMs highlighted in red represent the veto region, while those in blue define the fiducial volume. Events where the initial detected light comes from the veto region are excluded from the analysis. Figure taken from [19]	6
1.4	The neutrino effective areas for the high-energy starting event selection as a function of neutrino energy. The distributions are shown for all neutrino flavors, broken down by various zenith angle ranges.	7
1.5	The Atmospheric neutrino fluxes at $E_\nu = 10$ TeV. The plot shows the fraction of the flux that is not vetoed, known as passing fluxes (solid lines), alongside the total flux entering the detector (dashed lines) as a function of the cosine of the zenith angle. Figure is adapted from [24].	8
1.6	The atmospheric neutrino fluxes and the effect of self-vetoing are displayed for a neutrino energy level of $E_\nu = 100$ TeV, see caption of Figure 1.5. Figure taken from [24].	8
1.7	A sketch of energy asymmetry, it is a measure of the relative distribution of total deposited energy between the two cascades, as defined in 1.6. Sketch is adapted from [13].	11
1.8	A sketch of Energy Confinement, it is a measure of how confined are reconstructed energy depositions E_1 and E_2 are within their reconstructed vertices. The confinement, as shown in the sketch is checked within 40 m of the vertices. Sketch is adapted from [13].	12
1.9	The event classification scheme for the Ternary PID. The first level evaluates reconstruction quality; if the criteria are not met, events are classified as single cascades or tracks based on the likelihood values L_{monopod} and L_{SPE16} . The second level considers the reconstructed length, using a threshold below which distinct vertices of double cascades appear as a single cascade. The third and fourth levels focus on energy confinement and energy asymmetry, respectively. The last level is added to improve purity of the double cascade sample at high energies where misclassification is prominent due to glashow events.	13
1.10	Fraction of flavor content per bin in double cascade events. The left panel shows the distribution without the criteria of Total $E_{\text{deposited}} \geq 3$ PeV and $L_{\text{reco}} \leq 20$ m, indicating <i>purity contamination</i> at high energies from $\bar{\nu}_e$ Glashow events. The right panel presents the distribution after reclassifying double cascades as single cascades under these conditions.	14
1.11	The cross section for the Glashow resonance process $\nu_e + e^- \rightarrow W^- \rightarrow X$ is shown with and without initial state radiation and Doppler broadening. The black curve represents the cross section without these effects, the blue dotted curve includes initial state radiation, the orange dotted curve shows Doppler broadening, and the red curve combines both effects. Figure taken from [35].	15
1.12	Length Bias of true double cascades, classified as double cascades, as function of Azimuth angle. Vertical lines shows the direction of the major anisotropy axis. Caption below each figures shows which combination of icemode is used in simulation and reconstruction respectively. Each figure also shows reduced value of χ^2 calculated by fitting the showed horizontal line, see text for details.	17
1.13	Simulation using Spice-3.2.1 and reconstruction using Spice-3.2.1 but no effective distance. See caption of Figure 1.12 for details.	18

2.1	Figure depicts the proposed IceCube-Gen2 Neutrino Observatory facility at the South Pole. It includes (from left to right) (i) a radio array with 200 stations, (ii) 120 new in-ice strings, spaced 240 m apart (shown as orange points), as an expansion of (iii) current optical array, (iv) 7 strings of IceCube upgrade, to be deployed soon within current in-ice DeepCore volume. Figure taken from [40]	19
2.2	The designs of the IceCube-Gen2 optical sensors, DOM-16(second) and DOM-18 (third) with their base designs, to be used in the IceCube Upgrade sensors, are the mDOM on the left and D-Egg on the right [46]	20
2.3	The effective area is compared for IceCube-Gen2 DOM candidates, 16, and 18 PMT models, in relation to IceCube-Gen1 DOM (pDOM), D-Egg, and mDOM, as functions of zenith angle (left) and wavelength averaged over solid angle (right). Figure taken from [46]	22
2.4	Conceptual representation of Simulated sensor with isotropic angular acceptance (iso-pDOM)	22
2.5	Results of simulating a sensor that <i>mimics</i> the behaviour of a typical mDOM. The blue line shows changed effective area of the so-called <i>isopDOM</i> , achieved by combining acceptance curves of pDOMs having a PMT in "upper" (orange) and "lower" (grey) halves of the DOM respectively	22
2.6	2D Monte Carlo templates, constructed using reconstructed total energy (E_{Tot}) and double cascade length (L_{dc}) for events classified as double cascades . The signal (left), representing ν_{τ} -induced double cascades, shows a clear correlation between L_{dc} and E_{tot} . In contrast, the background (right), consisting of ν_{μ} and ν_e events, lacks this correlation and clusters at low L_{dc}	23
2.7	Selection Efficiency : Ratio of neutrinos that got classified into a topology to all the neutrinos that interacted in active volume. Data here refers to monte-carlo events per energy bin.	25
2.8	Classification Efficiency: Three subplot columns are true neutrino flavours, where each energy bin (true Monte Carlo energy) contains the fraction of topologies, summing to 100%. Diagonal plots show the flavour identification efficiency of the classifier, whereas off-diagonal plots show misidentification fractions.	26
2.9	Projected sensitivity of IceCube-Gen2 to measure flavour composition of Astrophysical neutrino with 10 years of its lifetime. The maroon line shows sensitivity using the ternary classification scheme and light salmon shade shows sensitivity without a dedicated ν_{τ} identifier. The unresolved degeneracy along ν_e/ν_{τ} axis is notable due to lack of double cascade classifier. The solid (dashed) lines depict the corresponding 68% (99%) constraints, derived assuming Wilks' theorem.	27
2.10	The bottom section displays the proportion of ν_{μ} at the source based on energy, with the assumption that the muon critical energy is 2 PeV. The error bars represent the 68% confidence level limitations on the ν_{μ} fraction below and above 1 PeV, derived from the observed flavour composition of ν_{μ} at Earth using IceCube-Gen2 and assuming standard oscillations. In the upper sections, the dark (light) shaded regions depict the corresponding 68% (99%) constraints, without making any assumptions about the mixing matrix.	28
2.11	A combined sensitivity to measure evolution of the neutrino flavour composition with energy ranges from TeV to EeV range, using both optical and radio components of IceCube Gen2 Detector. Astrophysical neutrino sources are generally expected to be dominated by pion decay at the lowest energies, with a flavour composition of approximately (1:2:0). At intermediate energies, the sources transition to a muon-damped production regime, yielding a flavour ratio of roughly (0:1:0). Finally, at the highest energies, the composition reverts to the pion decay pattern, (1:1:1), as anticipated for cosmogenic neutrino production. The details for layout are similar to that shown in Figure 2.10. The extended figure, taken from [52].	29

List of Tables

1.1 The four comparison scenarios that were analyzed. The First icemodel in the name always refers to the one used in simulation (second column) and the second refers to the one used in reconstruction (reconstruction). Last column points to corresponding figures.	17
---	----

Bibliography

Here are the references in citation order.

- [1] A. M. Dziewonski and D. L. Anderson. "Preliminary reference earth model". In: *Phys. Earth Planet. Interiors* 25 (1981), pp. 297–356. doi: [10.1016/0031-9201\(81\)90046-7](https://doi.org/10.1016/0031-9201(81)90046-7) (cited on page 2).
- [2] F. Halzen and D. Saltzberg. "Tau-neutrino appearance with a 1000 megaparsec baseline". In: *Physical Review Letters* 81 (1998), pp. 4305–4308 (cited on page 2).
- [3] D. Heck et al. "CORSIKA: A Monte Carlo code to simulate extensive air showers". In: (Feb. 1998) (cited on page 2).
- [4] J. van Santen. "Neutrino Interactions in IceCube above 1 TeV: Constraints on Atmospheric Charmed-Meson Production and Investigation of the Astrophysical Neutrino Flux with 2 Years of IceCube Data taken 2010–2012". PhD thesis. Wisconsin U., Madison, Nov. 2014 (cited on pages 3, 9).
- [5] J. H. Koehne et al. "PROPOSAL: A tool for propagation of charged leptons". In: *Comput. Phys. Commun.* 184 (2013), pp. 2070–2090. doi: [10.1016/j.cpc.2013.04.001](https://doi.org/10.1016/j.cpc.2013.04.001) (cited on page 4).
- [6] D. Chirkov and W. Rhode. "Propagating leptons through matter with Muon Monte Carlo (MMC)". In: (Aug. 2004) (cited on page 4).
- [7] B. Voigt. "Sensitivity of the IceCube detector for ultra-high energy electron-neutrino events". PhD thesis. Humboldt-Universität zu Berlin, Mathematisch-Naturwissenschaftliche Fakultät I, 2008. doi: <http://dx.doi.org/10.18452/15850> (cited on page 4).
- [8] L. Radel and C. Wiebusch. "Calculation of the Cherenkov light yield from electromagnetic cascades in ice with Geant4". In: *Astropart. Phys.* 44 (2013), pp. 102–113. doi: [10.1016/j.astropartphys.2013.01.015](https://doi.org/10.1016/j.astropartphys.2013.01.015) (cited on page 4).
- [9] L. Rädel and C. Wiebusch. "Calculation of the Cherenkov light yield from low energetic secondary particles accompanying high-energy muons in ice and water with Geant 4 simulations". In: *Astroparticle Physics* 38 (June 2012) (cited on page 4).
- [10] C. Kopper. *Photons from IceCube Muon*. URL: <https://www.psu.edu/news/research/story/national-science-foundation-funds-supercomputer-cluster-penn-state> (cited on page 4).
- [11] C. Kopper. *Clsim*. URL: <https://github.com/claudiok/clsim> (cited on page 4).
- [12] D. Chirkov. "Photon tracking with GPUs in IceCube". In: *Nuclear Instruments and Methods in Physics Research Section A: Accelerators, Spectrometers, Detectors and Associated Equipment* 725 (2013), pp. 141–143. doi: <https://doi.org/10.1016/j.nima.2012.11.170> (cited on page 4).
- [13] M. Usner. "Search for Astrophysical Tau-Neutrinos in Six Years of High-Energy Starting Events in the IceCube Detector". PhD thesis. Humboldt-Universität zu Berlin, Mathematisch-Naturwissenschaftliche Fakultät, 2018. doi: <http://dx.doi.org/10.18452/19458> (cited on pages 5, 8, 10–12, 14, 16, 18).
- [14] N. Whitehorn, J. van Santen, and S. Lafebre. "Penalized splines for smooth representation of high-dimensional Monte Carlo datasets". In: *Computer Physics Communications* 184.9 (2013), pp. 2214–2220. doi: <https://doi.org/10.1016/j.cpc.2013.04.008> (cited on pages 5, 8).
- [15] R. Abbasi et al. "Calibration and characterization of the IceCube photomultiplier tube". In: *Nuclear Instruments and Methods in Physics Research Section A: Accelerators, Spectrometers, Detectors and Associated Equipment* 618.1 (2010), pp. 139–152. doi: <https://doi.org/10.1016/j.nima.2010.03.102> (cited on page 5).
- [16] M. G. Aartsen et al. "Efficient propagation of systematic uncertainties from calibration to analysis with the SnowStorm method in IceCube". In: *JCAP* 10 (2019), p. 048. doi: [10.1088/1475-7516/2019/10/048](https://doi.org/10.1088/1475-7516/2019/10/048) (cited on page 5).

- [17] E. Ganster. "Measurement of the high-energy astrophysical neutrino energy spectrum combining muon tracks and cascades measured at the IceCube Neutrino Observatory". PhD thesis. RWTH Aachen University, RWTH Aachen U., 2024 (cited on page 6).
- [18] R. Naab. "Evidence for a Break in the Diffuse Extragalactic Neutrino Spectrum". PhD thesis. Humboldt-Universität zu Berlin, Mathematisch-Naturwissenschaftliche Fakultät, 2024 (cited on page 6).
- [19] R. Abbasi et al. "IceCube high-energy starting event sample: Description and flux characterization with 7.5 years of data". In: *Physical Review D* 104.2 (2021). doi: [10.1103/physrevd.104.022002](https://doi.org/10.1103/physrevd.104.022002) (cited on pages 6, 8, 23).
- [20] M. G. Aartsen et al. "Evidence for High-Energy Extraterrestrial Neutrinos at the IceCube Detector". In: *Science* 342.6161 (2013), p. 1242856. doi: [10.1126/science.1242856](https://doi.org/10.1126/science.1242856) (cited on page 6).
- [21] R. Abbasi et al. "Detection of astrophysical tau neutrino candidates in IceCube". In: *The European Physical Journal C* 82.11 (2022). doi: [10.1140/epjc/s10052-022-10795-y](https://doi.org/10.1140/epjc/s10052-022-10795-y) (cited on pages 6, 10, 23).
- [22] M. G. Aartsen et al. "Atmospheric and astrophysical neutrinos above 1 TeV interacting in IceCube". In: *Phys. Rev. D* 91 (2 Jan. 2015), p. 022001. doi: [10.1103/PhysRevD.91.022001](https://doi.org/10.1103/PhysRevD.91.022001) (cited on page 7).
- [23] V. Basu et al. "From PeV to TeV: Astrophysical Neutrinos with Contained Vertices in 10 years of IceCube Data". In: *PoS ICRC2023* (2023), p. 1007. doi: [10.22323/1.444.1007](https://doi.org/10.22323/1.444.1007) (cited on page 7).
- [24] C. Arguelles Delgado et al. "Unified atmospheric neutrino passing fractions for large-scale neutrino telescopes". In: *Journal of Cosmology and Astroparticle Physics* 2018 (July 2018), pp. 047–047. doi: [10.1088/1475-7516/2018/07/047](https://doi.org/10.1088/1475-7516/2018/07/047) (cited on pages 7, 8).
- [25] T. Yuan et al. *nuVeto*. URL: <https://github.com/tianluyuan/nuVeto> (cited on page 8).
- [26] A. Fedynitch et al. "Calculation of conventional and prompt lepton fluxes at very high energy". In: *EPJ Web Conf.* 99 (2015). Ed. by D. Berge et al., p. 08001. doi: [10.1051/epjconf/20159908001](https://doi.org/10.1051/epjconf/20159908001) (cited on page 8).
- [27] M. G. Aartsen et al. "Energy Reconstruction Methods in the IceCube Neutrino Telescope". In: *JINST* 9 (2014), P03009. doi: [10.1088/1748-0221/9/03/P03009](https://doi.org/10.1088/1748-0221/9/03/P03009) (cited on pages 8, 16).
- [28] T. Yuan. "Detecting neutrinos in IceCube with Cherenkov light in the South Pole ice". In: *Nucl. Instrum. Meth. A* 1054 (2023), p. 168440. doi: [10.1016/j.nima.2023.168440](https://doi.org/10.1016/j.nima.2023.168440) (cited on page 8).
- [29] R. Abbasi et al. "In situ estimation of ice crystal properties at the South Pole using LED calibration data from the IceCube Neutrino Observatory". In: *The Cryosphere* 18.1 (2024), pp. 75–102. doi: [10.5194/tc-18-75-2024](https://doi.org/10.5194/tc-18-75-2024) (cited on page 9).
- [30] J. Stachurska. "Astrophysical Tau Neutrinos in IceCube". PhD thesis. Humboldt-Universität zu Berlin, Mathematisch-Naturwissenschaftliche Fakultät, 2020. doi: <http://dx.doi.org/10.18452/21611> (cited on pages 11, 14, 16).
- [31] A. Cooper-Sarkar, P. Mertsch, and S. Sarkar. "The high energy neutrino cross-section in the Standard Model and its uncertainty". In: *JHEP* 08 (2011), p. 042. doi: [10.1007/JHEP08\(2011\)042](https://doi.org/10.1007/JHEP08(2011)042) (cited on page 14).
- [32] S. L. Glashow. "Resonant Scattering of Antineutrinos". In: *Phys. Rev.* 118 (1 Apr. 1960), pp. 316–317. doi: [10.1103/PhysRev.118.316](https://doi.org/10.1103/PhysRev.118.316) (cited on page 14).
- [33] D. Garg et al. "Neutrino propagation in the Earth and emerging charged leptons with nuPyProp". In: *JCAP* 01 (2023), p. 041. doi: [10.1088/1475-7516/2023/01/041](https://doi.org/10.1088/1475-7516/2023/01/041) (cited on page 15).
- [34] C. A. Argüelles et al. "Tau depolarization at very high energies for neutrino telescopes". In: *Phys. Rev. D* 106.4 (2022), p. 043008. doi: [10.1103/PhysRevD.106.043008](https://doi.org/10.1103/PhysRevD.106.043008) (cited on page 15).
- [35] G.-y. Huang, M. Lindner, and N. Volmer. "Inferring astrophysical neutrino sources from the Glashow resonance". In: *JHEP* 11 (2023), p. 164. doi: [10.1007/JHEP11\(2023\)164](https://doi.org/10.1007/JHEP11(2023)164) (cited on pages 15, 16).
- [36] A. Garcia et al. "Complete predictions for high-energy neutrino propagation in matter". In: *JCAP* 09 (2020), p. 025. doi: [10.1088/1475-7516/2020/09/025](https://doi.org/10.1088/1475-7516/2020/09/025) (cited on page 15).

- [37] R. Gauld. "Precise predictions for multi-TeV and PeV energy neutrino scattering rates". In: *Phys. Rev. D* 100.9 (2019), p. 091301. doi: [10.1103/PhysRevD.100.091301](https://doi.org/10.1103/PhysRevD.100.091301) (cited on page 15).
- [38] A. Loewy, S. Nussinov, and S. L. Glashow. "The Effect of Doppler Broadening on the 6.3 PeV W^- Resonance in $\bar{\nu}_e e^-$ Collisions". In: (July 2014) (cited on pages 15, 16).
- [39] D. Chirkin and IceCube Collaboration. "Evidence of optical anisotropy of the South Pole ice". In: *International Cosmic Ray Conference*. Vol. 33. International Cosmic Ray Conference. Jan. 2013, p. 3338 (cited on page 16).
- [40] M. G. Aartsen et al. "IceCube-Gen2: the window to the extreme Universe". In: *Journal of Physics G: Nuclear and Particle Physics* 48.6 (2021), p. 060501. doi: [10.1088/1361-6471/abbd48](https://doi.org/10.1088/1361-6471/abbd48) (cited on pages 19, 20).
- [41] A. Ishihara. "The IceCube Upgrade - Design and Science Goals". In: *PoS ICRC2019* (2021), p. 1031. doi: [10.22323/1.358.1031](https://doi.org/10.22323/1.358.1031) (cited on page 19).
- [42] IceCube Collaboration and F. Schröder. *IceCube-Gen2 Surface Array: Science Case and Plans*. Vortrag gehalten auf DPG Frühjahrstagung: Fachverband Teilchenphysik (2024), Karlsruhe, Deutschland, 4.–8. März 2024. 51.13.04; LK 01. 2024 (cited on page 19).
- [43] G. A. Askar'yan. "Excess negative charge of an electron-photon shower and its coherent radio emission". In: *Zh. Eksp. Teor. Fiz.* 41 (1961), pp. 616–618 (cited on page 20).
- [44] Z. S. Meyers et al. *Radio Detection of EeV Neutrinos in Dielectric Media using the Askaryan Effect* *for Babies*. DESY, 2021, pp. 1–14 (cited on page 20).
- [45] J. A. Aguilar et al. "The Next-Generation Radio Neutrino Observatory – Multi-Messenger Neutrino Astrophysics at Extreme Energies". In: (July 2019) (cited on page 20).
- [46] R. "Abbasi and others". *The IceCube Gen2 Technical Design Report*. https://icecube-gen2.wisc.edu/wp-content/uploads/2023/07/IceCube_Gen2_TDR_0.05_July27.2023_Part_I_and_II.pdf. [Accessed 18-06-2024]. 2023 (cited on pages 20–22, 28).
- [47] L. Classen et al. "The mDOM - A multi-PMT digital optical module for the IceCube-Gen2 neutrino telescope". In: *PoS ICRC2017* (2017), p. 1047. doi: [10.22323/1.301.1047](https://doi.org/10.22323/1.301.1047) (cited on page 21).
- [48] L. Classen et al. "A multi-PMT Optical Module for the IceCube Upgrade". In: *PoS ICRC2019* (2019), p. 855. doi: [10.22323/1.358.0855](https://doi.org/10.22323/1.358.0855) (cited on page 21).
- [49] R. Abbasi et al. "D-Egg: a dual PMT optical module for IceCube". In: *JINST* 18.04 (2023), P04014. doi: [10.1088/1748-0221/18/04/P04014](https://doi.org/10.1088/1748-0221/18/04/P04014) (cited on page 21).
- [50] M. "Aartsen et al. "Letter of Intent: The Precision IceCube Next Generation Upgrade (PINGU)". In: *E-Print: arXiv* 1401.2046 [physics.ins-det] (Jan. 2014) (cited on page 21).
- [51] A. Omeliukh. "Optimization of the optical array geometry for IceCube-Gen2". Master's thesis. Kyiv, Ukraine: Taras Schevchenko national University of Kyiv, 2021 (cited on page 22).
- [52] A. Coleman et al. "The flavor composition of ultra-high-energy cosmic neutrinos: measurement forecasts for in-ice radio-based EeV neutrino telescopes". In: (Feb. 2024) (cited on pages 24, 28, 29).
- [53] J. van Santen et al. "toise: a framework to describe the performance of high-energy neutrino detectors". In: *Journal of Instrumentation* 17.08 (2022), T08009. doi: [10.1088/1748-0221/17/08/t08009](https://doi.org/10.1088/1748-0221/17/08/t08009) (cited on page 24).
- [54] R. Abbasi et al. "Improved Characterization of the Astrophysical Muon–neutrino Flux with 9.5 Years of IceCube Data". In: 928.1 (2022), p. 50. doi: [10.3847/1538-4357/ac4d29](https://doi.org/10.3847/1538-4357/ac4d29) (cited on page 26).
- [55] N. Lad et al. "Summary of IceCube tau neutrino searches and flavor composition measurements of the diffuse astrophysical neutrino flux". In: *PoS ICRC2023* (2023), p. 1122. doi: [10.22323/1.444.1122](https://doi.org/10.22323/1.444.1122) (cited on page 26).
- [56] N. Lad et al. "Sensitivity of IceCube-Gen2 to measure flavor composition of Astrophysical neutrinos". In: *PoS ICRC2023* (2023), p. 1123. doi: [10.22323/1.444.1123](https://doi.org/10.22323/1.444.1123) (cited on page 27).

- [57] G. Cowan et al. "Asymptotic formulae for likelihood-based tests of new physics". In: *Eur. Phys. J. C* 71 (2011). [Erratum: Eur.Phys.J.C 73, 2501 (2013)], p. 1554. doi: [10.1140/epjc/s10052-011-1554-0](https://doi.org/10.1140/epjc/s10052-011-1554-0) (cited on page 27).
- [58] M. G. Aartsen et al. "A combined maximum-likelihood analysis of the high-energy astrophysical neutrino flux measured with IceCube". In: *Astrophys. J.* 809.1 (2015), p. 98. doi: [10.1088/0004-637X/809/1/98](https://doi.org/10.1088/0004-637X/809/1/98) (cited on page 27).
- [59] S. S. Wilks. "The Large-Sample Distribution of the Likelihood Ratio for Testing Composite Hypotheses". In: *Annals Math. Statist.* 9.1 (1938), pp. 60–62. doi: [10.1214/aoms/1177732360](https://doi.org/10.1214/aoms/1177732360) (cited on page 27).
- [60] T. Kashti and E. Waxman. "Astrophysical Neutrinos: Flavor Ratios Depend on Energy". In: *Phys. Rev. Lett.* 95 (18 Oct. 2005), p. 181101. doi: [10.1103/PhysRevLett.95.181101](https://doi.org/10.1103/PhysRevLett.95.181101) (cited on page 27).
- [61] W. Winter. "Describing the Observed Cosmic Neutrinos by Interactions of Nuclei with Matter". In: *Phys. Rev. D* 90.10 (2014), p. 103003. doi: [10.1103/PhysRevD.90.103003](https://doi.org/10.1103/PhysRevD.90.103003) (cited on page 28).
- [62] M. Bustamante, J. F. Beacom, and W. Winter. "Theoretically Palatable Flavor Combinations of Astrophysical Neutrinos". In: *Phys. Rev. Lett.* 115 (16 Oct. 2015), p. 161302. doi: [10.1103/PhysRevLett.115.161302](https://doi.org/10.1103/PhysRevLett.115.161302) (cited on page 28).